Quantifying the Energetic Costs of Photovoltaic Pumping Systems (PVPS) for Sub-Saharan African Smallholder Farms

by

ZhiYi Liang

B.S. Mechanical Engineering, Massachusetts Institute of Technology (2019)

Submitted to the Department of Mechanical Engineering
in partial fulfillment of the requirements for the degree of

Master of Science in Mechanical Engineering

at the

MASSACHUSETTS INSTITUTE OF TECHNOLOGY

June 2021

Author . . . . . .
Department of Mechanical Engineering
May 14, 2021

Certified by . . . . . .
Amos G. Winter, V
Associate Professor of Mechanical Engineering
Thesis Supervisor

Accepted by . . . . . .
Nicolas Hadjiconstantinou
Professor of Mechanical Engineering
Graduate Officer

Quantifying the Energetic Costs of Photovoltaic Pumping Systems (PVPS) for Sub-Saharan African Smallholder Farms

by

ZhiYi Liang

Submitted to the Department of Mechanical Engineering
on May 14, 2021, in partial fulfillment of the
requirements for the degree of
Master of Science in Mechanical Engineering

Abstract

With the solar panel prices falling recently, photovoltaic pumping systems (PVPSs) have become an affordable and effective technology for off-grid smallholder farmers in developing markets like Sub-Saharan Africa. Yet the high upfront cost of PVPSs remains a financial burden for many low-income farming communities. Although numerous efforts have been made to further increase the affordability of PVPSs, there is still a lack of investigation into potential energetic cost savings by improving solar pump efficiency from an architectural design perspective. In this study, a technoeconomic framework was developed to quantify the energetic costs of different solar pump architectures. The energetic cost is defined as the total cost of the solar array, which enables a direct comparison between efficiency and capital cost. New efficiency prediction models were formulated for 4-inch borehole pump hydraulics and submersible motors based on surveyed manufacturer specifications. Two types of case studies on SSA farms were conducted as example analyses in applying the framework. The operating space level analysis provides a bird's-eye view of the energetic cost-savings over the operating space when comparing two solar pump architectures. The operating point level analysis demonstrates a similar energetic cost analysis to identify the most energetically cost-effective solar pump architectures for the operating conditions of a specific SSA farm. By adopting highly efficient BLDC motors in 4-inch solar-powered borehole pumps, energetic cost-savings were found and operating regions not currently served by high-efficiency solar pumps can now be reached. These results highlight economic incentives for manufacturers to provide high-efficiency solar pumps to more smallholder farmers in SSA while reducing the overall upfront cost of PVPSs.

Thesis Supervisor: Amos G. Winter, V
Title: Associate Professor of Mechanical Engineering

Acknowledgments

I would like to take the time to acknowledge and thank the following groups of people for supporting me throughout my work:

- First and foremost, I would like to thank my graduate advisor, Professor Amos Winter, for his continued support throughout this project and the genuine advice that helped me grow both professionally and personally. Thank you, Amos!

- Secondly, I would like to acknowledge the drip irrigation team at the GEAR Lab. This work could not have been done without the collaborative efforts of the members of the team. In addition, I would also like to thank members from the rest of the GEAR Lab, it has been a great experience working with you and getting to know you. So, thank you all!

- I would like to acknowledge Xylem Inc. for funding this project, Jeff Lopes and his colleagues for the collaborative supports throughout this research. I would also like to acknowledge NSF GRFP for providing the additional funding for this project.

- I would like to express my gratitude to my parents, family, and friends. Thank you for your support and encouragement during these years as I am grinding for more degrees. *(By the way, Alex that is a cool mill you got there! Alvaro and Bryan, I hope $GME will take you to the moon. Oh yes, Valentino and John, you guys need to get some sleep, Ph.D. is a marathon man.)*

- Last but not least, this is unrelated to this work but I just want to take the chance to thank everyone around the world who has contributed to the combined efforts of defeating COVID-19. This historical pandemic has shown a lot of good and bad about our society, but I am faithful that humanity will do what is right in the face of challenging times.

Contents

List of Figures

List of Tables

Chapter 1

Introduction

1.1 Motivation

Recently, there has been a growing interest to provide low-cost photovoltaic pumping systems (PVPSs) to increase reliable water access for the estimated 50 million smallholder farmers in Sub-Saharan Africa (SSA), who collectively produce more than 80% of the food for the region [22, 17]. Studies have shown that increasing reliable water access is an effective tool to alleviate poverty and strengthen food security, particularly for smallholder farmers [3, 13]. With the abundance of groundwater at shallow depths, SSA is suitable for installing electric groundwater pumps to provide reliable water access and improve the livelihood of rural households [23, 29]. However, many of the smallholder farmers are off-grid, forcing them to rely on inefficient diesel-powered pumps with high recurring fuel costs [6]. While the price of solar panels has rapidly declined in recent years, falling from 21 USD/W_p [1] in 1992 to 0.81 USD/W_p as of 2019 [20, 8], solar-electric systems are becoming more cost-competitive with diesel-powered systems because the lifetime cost of diesel fuel has started to outweigh the high upfront cost of the solar array [6]. However, many smallholders remain financially hesitant to purchase PVPSs since they are more sensitive to the high upfront cost of PVPS than the high lifetime cost of diesel fuel, creating a barrier of wide-scale adoption for PVPSs in the region [30].

[1] Solar panels have power specifications in watt-peak (W_p), which is the peak electrical power generation under optimal conditions. The unit USD/W_p represents the US dollar amount retail price per watt-peak of solar panels.

1.2 Previous Work and Knowledge Gaps

To increase the affordability of PVPSs, numerous efforts have been made in the past decade to understand the current state of PVPS technologies and develop a wide variety of cost-saving strategies. When reviewing the current state of PVPS technologies worldwide, Chandel et al. [5] identified the key strategies to reduce the high upfront cost of PVPSs are through government incentives and efficiency improvements. By increasing the efficiency of PVPSs, a large reduction in upfront cost can be achieved since the solar array is often sized based on the total efficiency of the system and it is generally the dominating cost factor [24]. With advancements in PV cell technologies, the efficiency of both commercial silicon and thin-film solar cells has increased 4% over the past decade and their cost of manufacturing has fallen 90% since the 1970s [5]. Researchers have also found experimentally that cooling the panel surface with sprayed water during system operation can effectively increase panel efficiency by more than 3% [1]. Moreover, engineers have developed increasingly sophisticated maximum power point tracking (MPPT) algorithms over the commonly used perturb-and-observe method, further increasing panel output efficiency for PVPSs at the cost of additional computational complexity [18].

In addition to improving PV efficiency, motor power savings of 8% can be achieved by implementing minimal loss point tracking (MLPT) for solar pump motors in conjunction with MPPT for the solar array [9]. From the power electronic perspective, a newly designed low-cost, high-efficiency solar pump driver can achieve a peak efficiency of 93.64% at 0.43 USD/W_p, reducing the electronic component cost and making PVPS more affordable in developing markets [4]. In hardware, Sashidhar et al. [33] designed a low-cost high-efficiency borehole motor with a predicted efficiency of 88% using ferrite magnets, enabling a potential cost-competitive alternative to both rare-earth magnet motors and induction motors.

When designing PVPSs for irrigation-specific applications, researchers have developed a system optimization model based on numerical sizing methods using the loss of load probability (LLP) to achieve low system cost while guaranteeing system reliability on crop yield [35]. In addition, newly designed ultra-low-pressure pressure-compensating

drippers can further increase energy efficiency by maintaining required pumping power and the volume of water required to irrigate, providing additional cost-savings for solar-powered irrigation systems [34]. However, while prior art provides multiple avenues to improve PVPS efficiency and increase affordability, only a limited amount has been done to investigate the potential impact of efficiency improvement from a solar pump architecture design standpoint – which considers the pump hydraulic body and the submersible motor. There is also a lack of quantification on the cost implication that arises from the inefficiency of the solar pumps, especially from an operating space-wide perspective, in which the operating space is defined as the flow-rate pressure (Q-H) hydraulic operating plane.

While the solar pump is the primary energy consumer in a PVPS, improving its efficiency can lead to potential cost savings on the overall system. Extra solar panels are required to compensate for the power losses through the pump hydraulics and the motor, incurring additional upfront costs on the PVPS. The upfront cost of the solar array is defined as the energetic cost in this thesis, which is attributed to the operating hydraulic power and the inefficiency of the solar pump. Energetic cost-savings exist when considering solar pump architectures with higher efficiency pump hydraulic and motor options. These energetic cost-savings can be compared with the potential capital cost premiums of the more efficient solar pump component options, providing a useful indicator for evaluating the overall solar pump architecture cost-effectiveness. However, existing sizing software from prominent pump manufacturers, such as Grundfos, Xylem, and Lorentz, are unable to provide an energetic cost comparison between solar pump architectures [14, 38, 21]. These sizing software packages were developed with the intent to design a PVPS for specific operating conditions given the companies' already existing product portfolio. Therefore, a technoeconomic framework that characterizes the efficiency performance and quantifies the associated energetic costs of different solar pump architectures can be beneficial for both solar pump manufacturers and PVPS designers. It allows manufacturers and system designers to formulate direct trade-off comparisons between efficiency benefits and capital cost premiums when selecting hardware components to construct the optimal solar pump architecture.

To implement a framework that analyzes solar pump energetic costs, the efficiency performance of pump hydraulic and motor options need to be well-characterized and reliably

predicted. For the SSA market, 4-inch (101mm) diameter borehole pumps are one of the more commonly used groundwater lifting methods. This is because boreholes larger than 4 inches are uncommon in SSA due to the cost barrier of drilling and surface suction pumps are typically unable to reach a water depth of more than 7-10 meters without the risk of cavitation [28]. However, accurate efficiency characterizations for the 4-inch borehole pump hydraulics and motors are lacking in the operating space most relevant to the SSA irrigation market. Some statistical efficiency prediction laws exist [15, 2, 19], but they not adequate for the 4-inch borehole pump hydraulics on the current market (Section 3.1). Many theoretical design laws are also oriented toward developing a specific hardware design of certain geometry, which are unable to extrapolate efficiency predictions for the overall operating space [19, 15, 37, 26]. Therefore, the efficiency performance of 4-inch borehole pump hydraulics and motors need to be characterized and new efficiency prediction laws need to be formulated based on the efficiency characterizations.

1.3 Thesis Overview

This thesis presents a unique technoeconomic framework to quantify the efficiency-related energetic costs of different solar pump architectures. The efficiency performance of 4-inch borehole pump hydraulics and motors are characterized within the SSA irrigation space, by surveying published manufacturer specifications on commercially available products. New statistical prediction laws were formulated to predict the efficiency performance of the commonly used 4-inch multistage centrifugal pump (MSP) hydraulic and progressive cavity pump (PCP) hydraulics (Section 3.1). Statistical prediction laws for commonly used 4-inch submersible AC induction motors (IMs) were also formulated. The IEC 60034-30-1:2014 international motor efficiency standard was used to represent highly efficient motors, such as permanent magnet brushless DC motors (PM-BLDC) (Section 3.2). The total efficiency and volumetric specific energy of 10 solar pump architectures were explored as a function of flow rate and pressure over the hydraulic operating space using the efficiency prediction models. The energetic costs were calculated using the technoeconomic framework for the solar pump architectures of interest in the SSA farm case studies.

Two case studies were conducted for SSA farms to demonstrate the application of the energetic cost framework: 1) an operating space-level analysis, and 2) an operating point-level analysis. On the operating space level, the simulated results provide a bird's-eye view of the quantifiable energetic cost-savings between two solar pump architectures over the hydraulic operating space. It highlights regions in the operating space where economic incentives are pronounced for manufacturers to adopt the more efficient solar pump architecture. Manufacturers can directly weigh the energetic cost-savings simulated by the framework against the capital costs premiums of the more efficient hardware. By incorporating the energetic cost framework, manufacturers can better understand the cost implications of efficiency to design more cost-effective solar pumps for the various SSA operating regions. On the operating point level, the framework is used to compare the energetic costs of multiple solar pump architectures viable for the specific operating conditions of an SSA farm. The ability to generate cross-architectural comparisons allows PVPS designers to identify the most energetically cost-effective architectures and make informed technoeconomic decisions in their system design process. Both of these case studies provide an example of how industrial practitioners can use the described framework in their design process to evaluate the efficiency-related cost implications of solar pump architectures, enabling them to provide more energy-efficient PVPSs to the cost-sensitive smallholder farmers in SSA at a more affordable price.

Chapter 2

Energetic Cost Framework Formulation

2.1 Overview of the Framework Structure

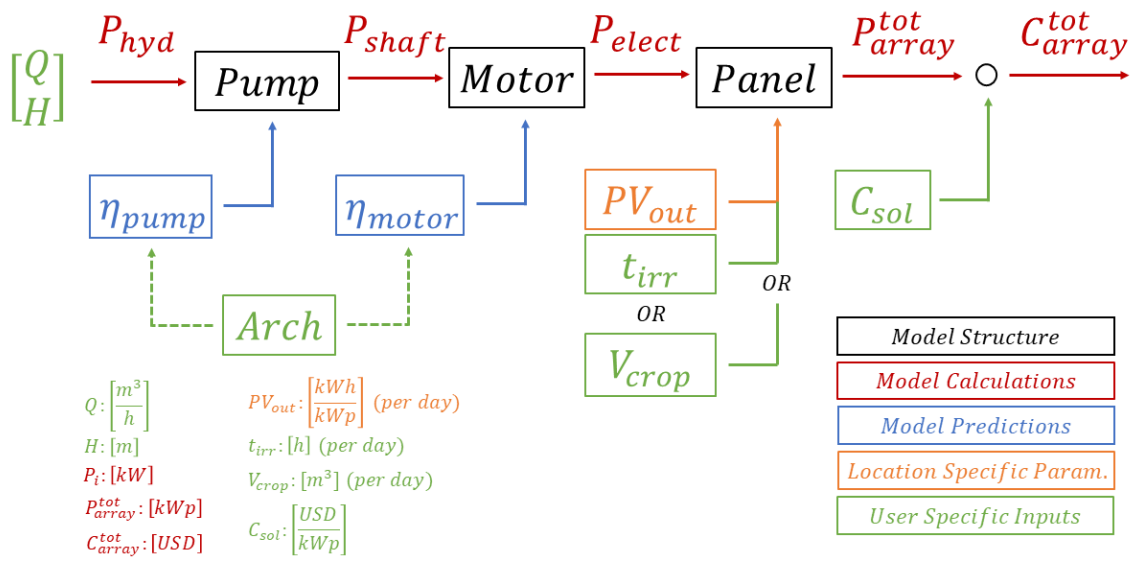

Fig. 2-1. Technoeconomic framework structure to quantify energetic costs of solar pump architectures.

The technoeconomic framework presented in this thesis quantifies the energetic cost-savings in terms of the difference in solar array upfront costs, between different solar pump architectures. The power flow into and out of each solar pump component is calculated based on the predicted efficiency of the component. The cost of the solar array is pro-

portional to its power, which is sized based on the total power requirement of the specific solar pump architecture. The term "architecture" includes two hardware components in a solar pump: the pump hydraulic body and the submersible motor. The framework model follows a backward power flow structure as shown in Fig. 2-1. Two parameters define the performance of a given solar pump architecture - the flow rate, Q $[m^3/h]$, and the operating pressure head, H $[m]$. The model first calculates the hydraulic power (P_{hyd}) based on the hydraulic operating flow rate and pressure using Eq. 2.1. The model then predicts the efficiency of the specified pump hydraulics (η_{pump}), in the architecture based on the hydraulic operating conditions. The efficiency prediction laws used to predict pump hydraulic body efficiency are newly formulated based on surveyed manufacturer specifications on commercially available 4-inch pump hydraulics. These new efficiency prediction laws for 4-inch borehole pump hydraulics are discussed more in-depth in Section 3.1.

$$P_{hyd} = Q \cdot H \tag{2.1}$$

After predicting the efficiency of the pump hydraulic body, the shaft power (P_{shaft}) is back-calculated using Eq. 2.2. The shaft power represents the mechanical power required as input to the pump hydraulic body and output from the submersible motor. Once the shaft power can be determined, the efficiency of the motor (η_{motor}) is calculated using efficiency prediction laws for 4-inch submersible motors. The efficiency predictions for 4-inch submersible motors are formulated based on surveyed 4-inch induction motor on the SSA market and the IE efficiency ratings [16]. The details of the efficiency prediction formulations for 4-inch submersible motors can be found in Section 3.2.

$$P_{shaft} = \frac{P_{hyd}}{\eta_{pump}} \tag{2.2}$$

With the predicted motor efficiency, the electrical power (P_{elect}) required for the solar pump can be calculated from the shaft power using Eq. 2.3. The electrical power requirement is multiplied by a user input parameter of daily system run time to calculate the total daily electrical energy requirement E_{elect} used by the specific solar pump architecture. Since this study focuses on irrigation as an example application of PVPSs, the system run

time is defined as the time of irrigation t_{irr}. The total power of the solar array (P^{tot}_{array}) can then be sized using a location-specific daily average PV output potential PV_{out} parameter provided by Global Solar Atlas [36], as shown in Eq. 2.4. The PV output potential has a unit of $[kWh/kW_p]$ and indicates the average electrical energy generation in kilowatt-hour (kWh) per kilowatt-peak (kW_p) of solar array installed at a specific geographical location. By sizing the solar array based on E_{elect} and PV_{out}, the framework assumed conservation of energy produced from the solar array, and the details of this assumption are discussed in the Section 2.2. The relevant solar GIS map on the modeled PV_{out} for Sub-Saharan Africa is reproduced in Appendix B. The associated total cost of the solar array (C^{tot}_{array}), or the energetic cost of the solar pump, is calculated as the product of the solar array power (P^{tot}_{array}) and the average solar panel retail price (C_{sol}) in the region, as shown in Eq. 2.5. The total cost of the solar array represents the energetic cost of the solar pump. The solar panel retail price used in this study is 810 USD/kW_p, which is a standard price reported locally in SSA [8].

$$P_{elect} = \frac{P_{shaft}}{\eta_{motor}} = \frac{P_{hyd}}{\eta_{pump} \cdot \eta_{motor}} \tag{2.3}$$

$$P^{tot}_{array} = \frac{E_{elect}}{PV_{out}} = \frac{P_{elect} \cdot t_{irr}}{PV_{out}} \tag{2.4}$$

$$C^{tot}_{array} = C_{sol} \cdot \frac{P_{elect} \cdot t_{irr}}{PV_{out}} \tag{2.5}$$

Once the total cost of the solar array is calculated, the energetic cost-savings between solar pump architectures with different efficiencies can be computed using Eq. 2.6. It is simply the difference in the total costs of the solar array between two solar pump architectures of interest. Intuitively, when comparing two solar pump architectures, the more efficient architecture will result in a lower solar array cost (energetic cost). Equivalently, the energetic cost-savings are the difference in solar array power between two solar pump architectures multiplied by the solar panel price. The percentage cost saving between two solar pump architectures can be calculated using Eq. 2.7.

$$\Delta C^{tot}_{array} = C^{tot}_{array}(arch_1) - C^{tot}_{array}(arch_2) \tag{2.6}$$

$$\Delta C^{tot}_{array}(\%) = \frac{C^{tot}_{array}(arch_1) - C^{tot}_{array}(arch_2)}{C^{tot}_{array}(arch_1)} \tag{2.7}$$

The total cost of the solar array associated with a specific solar pump architecture at a given location can be broken down into contributions from three individual components: the necessary hydraulic power (Eq. 2.8), the power required to compensate for the inefficiency in the pump hydraulics (Eq. 2.9), and the similar power losses due to inefficiency in the motor (Eq. 2.10). By breaking the energetic cost down into three corresponding components, it provides a more granular understanding of the dominant cost drivers and inefficiency contributions to the total energetic cost of a solar pump architecture. It also enables industrial practitioners to understand where energetic cost is most sensitive to the efficiency of the solar pump components in the different operating regions.

$$C^{hyd}_{array} = C_{sol} \cdot P^{tot}_{array} \cdot \eta_{tot} \tag{2.8}$$

$$C^{pump}_{array} = C_{sol} \cdot P^{tot}_{array} \cdot (\eta_{motor} - \eta_{tot}) \tag{2.9}$$

$$C^{motor}_{array} = C_{sol} \cdot P^{tot}_{array} \cdot (1 - \eta_{motor}) \tag{2.10}$$

The total efficiency can be used as a key metric to evaluate the energetic performance and quantify the efficiency-related costs of different solar pump architectures. It can be calculated using Eq. 2.11 as the product of the predicted pump hydraulic body efficiency and the motor efficiency. Equivalently, it also represents the ratio of the useful hydraulic power output from the pump to the electrical power input to the motor. The newly formulated efficiency prediction models presented in this thesis can predict the total efficiency of different solar pump architectures over the Q-H operating space. The total efficiency of the 10 solar pump architectures considered in the case studies is presented as results in Section 3.3.

$$\eta_{tot} = \frac{P_{hyd}}{P_{elect}} = \eta_{pump} \cdot \eta_{motor} \tag{2.11}$$

The volumetric specific energy (e_{sys}) defined in Eq. 2.12 is another important metric when evaluating the energetic-effectiveness of solar pumps and PVPS designs. It represents the electrical energy needed to deliver a cubic meter of water, given the efficiency performance of specific solar pump architecture. It highlights regions where the per-unit cost of water is most energetically expensive and per-unit cost-benefits from efficiency improvement is most pronounced in the operating space. The volumetric specific energy has a unit of $[kWh/m^3]$ and can be calculated by normalizing the electrical power requirement by the operating flow rate. The e_{sys} can also be used as an alternative parameter to size the solar array with the water volume demand as user input. For irrigation specific application, the water volume demands of a PVPS are specified by the crop water demand (V_{crop}), which is a daily volume (m^3/day) for a given farm area. The simulated volumetric specific energy of the 10 solar pump architectures considered in the case studies are presented as results in Section 3.4.

$$e_{sys} = \frac{P_{elect}}{Q} \tag{2.12}$$

With the calculated volumetric specific energy, Eq. 2.13 can be used to compute the total cost of the solar array for a solar pump architecture based on a specific irrigation volume demand. The formulation presented in Eq. 2.13 is a mathematically equivalent alternative to the previously presented Eq. 2.5 when calculating the total cost of the solar array. The difference is Eq. 2.5 uses t_{irr} as input requirement while V_{crop} is used in Eq. 2.13. The V_{crop} can be divided by Q to obtain t_{irr}.

$$C_{array}^{tot} = C_{sol} \cdot \frac{e_{sys} \cdot V_{crop}}{PV_{out}} \tag{2.13}$$

2.2 Framework Scope and Assumptions

The hydraulic operating space considered in this study is constructed based on the operating ranges of multistage centrifugal pump (MSP) and progressive cavity pump (PCP) hydraulics commonly used in 4-inch borehole pumps, which are popular in the SSA irrigation market. This hydraulic operating space has a flow rate ranging from 0.3 m^3/h to 18 m^3/h and pressure heads ranging from 10 m to 250 m (Sections 3.1). The operating space is found to overlap with the majority of the smallholder farm operating requirements based on previous studies and surveys conducted by the author's team. In SSA, the majority of the farm sizes are estimated to range from less than 1 Ha up to 5 Ha [22], with borehole depth ranges up to 300 m. However, the considered operating space only represents the spatial scope of the presented case study used to demonstrate the application of the framework. The energetic cost framework itself can be applied to other pump types, operating locations, and solar-powered applications.

In addition, the efficiency performance of the solar pumps is characterized in regards to their best efficiency points (BEPs) using benchmark market data. The benchmarking method provides an accurate reflection on the efficiencies of 4-inch borehole pumps currently accessible by the end-users. The BEP determines the hydraulic operating point where a motorized pump can achieve maximum efficiency by incorporating the operating efficiency characteristics of both the pump hydraulic and motor. The outputs of the framework are continuous, calculated as a function of BEP flow rate Q_{BEP} and BEP pressure H_{BEP}, in contrast to reality where a specific manufacturer may opt to commercialize the solar pumps at a set of discrete BEPs. A manufacturer may design and produce solar pumps at discrete BEP flow rates (e.g., 1 m^3/h, 3 m^3/h, and 5 m^3/h) due to design and logistical simplicity. In high-volume production, solar pump manufacturers are likely to produce a small set of pump designs with overlapping operating regions, allowing them to reduce the capital costs of tooling and molds. While the desired hydraulic operating point of a physical system may not always match exactly with the BEP, the actual efficiency can slightly deviate from the BEP efficiency. However, the deviation is expected to be small when compared to the inefficiencies of the solar pump hydraulic and motor.

The framework presented in this study relates the efficiency of solar pumps to the associated capital costs in the solar array, defined as the energetic cost. The formulation of the energetic cost enables direct comparison between the efficiency-related cost implications and the capital costs of the hardware components. However, capital costs are highly manufacturer-specific and location-dependent due to variations in labor cost, profit margin, supply chain complexity, and country duty policies. As a result, capital costs are hard to generalize and the scope of the framework is limited to providing the energetic cost quantification - which is dependent solely on the technical performance of the hardware components. When determining the overall cost-effectiveness of a solar pump architecture, engineers should formulate a trade-off analysis weighing the energetic cost-savings against the capital cost difference between hardware components of different efficiencies. If the energetic cost-savings outweigh the additional capital cost premiums of the more efficient hardware component (e.g. pump hydraulic or motor), the more efficient hardware component should be used in the solar pump architecture as it can result in a greater capital cost-saving to the overall solar-powered system.

When formulating the framework, assumptions were made to reduce the computational complexity. The framework was constructed based on the conservation of solar energy produced on a location-specific daily average. This assumes that the energy generated from the solar array can be fully buffered in a storage tank or batteries, and the energy can be transferred in a lossless manner through the system. In a physical system, energy losses can occur due to pipe friction or internal resistance in the batteries. These energy losses are expected to be minor when compared to the primary energy losses due to the inefficiency of the solar pump hydraulic and motor. Therefore, this is a valid assumption for this study which focuses on the energetic cost related to the efficiency performance of the solar pump.

In addition, the costs of the power electronics and batteries are not captured in this study. While the cost of these power system components can be correlated to the electrical power draw of the solar pump, which depends on its efficiency, the actual sizing of the components depends mostly on the setup and operation of the PVPS in the field. The layout of the power electronics is dependent on the electrical characteristics such as voltage and waveform requirements in an actual system. The battery size required in a PVPS is also

primarily dependent on the energy storage capacity threshold in the battery management algorithm and the amount of system run time after dark, in which both are set by the user. Therefore, the costs of the power system components are outside the scope of the presented framework and industrial practitioners may want to consider their cost associations when designing the actual system.

Chapter 3

Efficiency Characterization of 4-Inch Borehole Pumps

Table 3.1. Simulated 4-inch borehole pump architectures and the respective operating range.

Architectures	Motor	Hydraulic	Operating Range
IM* MSP	Induction Motor	Multistage Centrifugal	$7 < N_q < 100$ $1m^3/h < Q < 18m^3/h$ $10m < H < 250m$ $P_{shaft} > 0.12kW$
IE1 MSP	IE1 Motor		
IE2 MSP	IE2 Motor		
IE3 MSP	IE3 Motor		
IE4 MSP	IE4 Motor		
IM* PCP	Induction Motor	Progressive Cavity	$N_q < 10$ $0.3m^3/h < Q < 3.2m^3/h$ $10m < H < 250m$ $P_{shaft} > 0.12kW$
IE1 PCP	IE1 Motor		
IE2 PCP	IE2 Motor		
IE3 PCP	IE3 Motor		
IE4 PCP	IE4 Motor		

$*$ IM represents the surveyed 4-inch induction motors currently in the market.

In this chapter, efficiency characterizations for the 4-inch borehole MSP hydraulic, PCP hydraulic, and submersible IMs are presented. New efficiency prediction laws are formulated based on efficiency characterizations. IE motor efficiency ratings are used to represent higher efficiency motors such as PM-BLDC motors [16]. Total efficiency and volumetric specific energy of the 10 solar pump architectures listed in Table 3.1 are

calculated and presented as a function Q_{BEP} and H_{BEP} over the operating space. The presented results of η_{tot} and e_{sys} are generalizable for the 4-inch borehole pump architectures and are not location-dependent, since they are formulated based on only the hardware performance.

3.1 Efficiency Predictions for 4-Inch Borehole Pump Hydraulics

For the irrigation operating space in SSA, two types of pump hydraulic are commonly used to construct 4-inch borehole pumps: multistage centrifugal pumps (MSPs) and progressive cavity pumps (PCPs). These two pump hydraulics are appropriate for SSA irrigation space because they can fit into a 4-inch diameter form factor while meeting a range of flow rate and pressure requirements. MSPs are constructed with a series of stacked impeller-diffuser pairs in the pump hydraulic stage, typically mass-manufactured with stamped sheet metals or injection-molded plastic. In general, MSPs are designed for high flow rate applications. Pumped fluid in an MSP is moved by the radial motion in the impellers and the impellers are stacked to achieve a high-pressure head. On the other hand, PCPs are a type of positive displacement pump generally designed for high-pressure, low-flow applications. Fluid in a PCP is moved by a custom-machined helical rotor through a series of progressing cavities, producing high pressure with relatively high efficiency when compared to radial-motion pumps. However, due to the more sophisticated metal casting and CNC post-machining processes required to manufacture PCPs, they are generally more expensive than MSPs.

A fundamental parameter in pump design known as the specific speed is important when considering the efficiency performance and operating characteristics of a pump. Specific speed is used in the pump industry as an index for characterizing pump design. It encodes the operating regime, internal geometry, and the optimal operating condition [32]. The specific speed N_q defined in Eq. 3.1 is a function of rotor speed N, flow rate Q, and pressure head H measured at BEP. For MSPs, specific speed is calculated using impeller head-per-stage H_{st} [15], and the impeller becomes more radial as the specific speed decreases [19]. Here,

the European definition of the specific speed is used, with rotor speed is in rpm, the flow rate in m^3/s, and pressure head in m. The rotor speed of the pump is assumed to be 3000 rpm unless otherwise stated, based on the standard AC frequency used in SSA (50 Hz). For the pump hydraulics of interest, PCPs have a typical specific speed range of $2 < N_q < 10$, while MSPs have a higher and wider range of $7 < N_q < 100$ [15]. An overlapping operating region exists between these two hydraulics.

$$N_q = N(rpm) \cdot \frac{\sqrt{Q_(m^3/s)}}{H(m)^{3/4}} \tag{3.1}$$

3.1.1 Efficiency Prediction for Multistage Centrifugal Pump Hydraulic

To predict the efficiency of MSPs, Gülich [15] presented one of the published statistical efficiency prediction models. However, Gülich's formulation is only valid for pumps with a designed flow rate greater than 18 m^3/h (0.005 m^3/s). In this study, the MSPs on the 4-inch borehole pump market generally have a flow rates less than 18 m^3/h, where Gülich's model is invalid. In 1979, Anderson [2] published an efficiency prediction model for centrifugal pumps in a statistical study of over 15,000 pumps, with flow rates ranging from 1.44 m^3/h to $1.44 \cdot 10^6$ m^3/h ($4 \cdot 10^{-4}$ m^3/s to 400 m^3/s). The original Anderson model is shown in Eq. 3.2, which predicts centrifugal pump efficiency as a function of BEP flow rate in liter per second (1 l/s = 0.001 m^3/s) and the imperial specific speed N_s. The original Anderson model was modified by Karassik to more accurately reflect efficiency of pumps with $N_q > 44$ ($N_s > 2286$). The Anderson-Karassik model statistically predicts efficiency of MSP hydraulic as a function of three variables: BEP flow rate in gpm (1 $gpm = 6.3 \cdot 10^{-5}$ m^3/s), the specific speed (imperial definition), and rotor speed in rpm (assumed to be 3000). The Anderson-Karassik model is shown in Eq. 3.3 [19].

$$\eta_{pump}^{Anderson} = 0.94 - (13.2 \cdot Q(l/s))^{-0.32} - 0.29 \cdot \log_{10}(\frac{1400}{N_s})^2 \tag{3.2}$$

$$\eta_{pump}^{A-K} = 0.94 - 0.08955 \cdot (\frac{Q(gpm)}{N(rpm)})^{-0.21333} - 0.29 \cdot \log_{10}(\frac{2286}{N_s})^2 \tag{3.3}$$

The efficiency data of the 4-inch MSP hydraulics presented in Fig. 3-1 were collected from surveying four primary multistage centrifugal pump manufacturers in the Sub-Saharan African market. The surveyed MSP manufacturers are Grundfos, Lowara, Pedrollo, and CNP [14, 38, 31, 7]. The efficiency specifications are based on the published hydraulic testing results from the manufacturers. The data set shown contains 37 independent impeller designs that are used in 453 4-inch MSPs sold on the market. Impellers designed for a specific BEP flow rate can be stacked to create multiple pump models with different BEP pressures. Based on the surveyed data, 4-inch MSP hydraulics were found to have a BEP flow rate ranging from 1 m^3/h to 18 m^3/h and a pressure head up to 250 m. The BEP flow rate range and BEP pressure range define Q-H operating space for MSPs considered in this study. The MSPs that have the same impeller designs, but different numbers of impeller stages, are known to share similar BEP efficiencies when tested. This is because the majority of the hydraulic losses occur in the first 3 initial stages due to the flow entering in a nonlinear manner, and adding additional stages has minimal impact on the overall efficiency of the pump hydraulic (Praneetha Boppa and Kyle Schoenheit, Xylem engineers). Therefore, the total pressure head or the number of impeller stage do not influence the BEP efficiency of a MSP hydraulic body.

When compared to the surveyed efficiencies, it was found that both the Anderson and Anderson-Karassik efficiency prediction models were not accurate in predicting the efficiency of 4-inch MSP hydraulics, as shown in Fig. 3-1. The Anderson model underestimates efficiency performance while the Anderson-Karassik model overestimates. The two models result in a respective RMSE value of 14.3891 and 19.5488, respectively, when compared against the surveyed data. Two of the Anderson-Karassik model parameters, represented by C_1 and C_2 in Eq. 3.4, were refit to the surveyed data. From Fig. 3-1, it is clear that the refined GEAR Lab model (Eq. 3.4) with the refit parameters (Table 3.2) is a more accurate representation of the efficiencies (η_{pump}^{MSP}) for the surveyed 4-inch MSP hydraulics than the two preexisting models. The refined GEAR Lab model results in a better RMSE value of 6.4391. The values of the statistically fitted parameters and the corresponding RMSEs are presented in Table 3.2 for the Anderson-Karassik model and the refined GEAR Lab model.

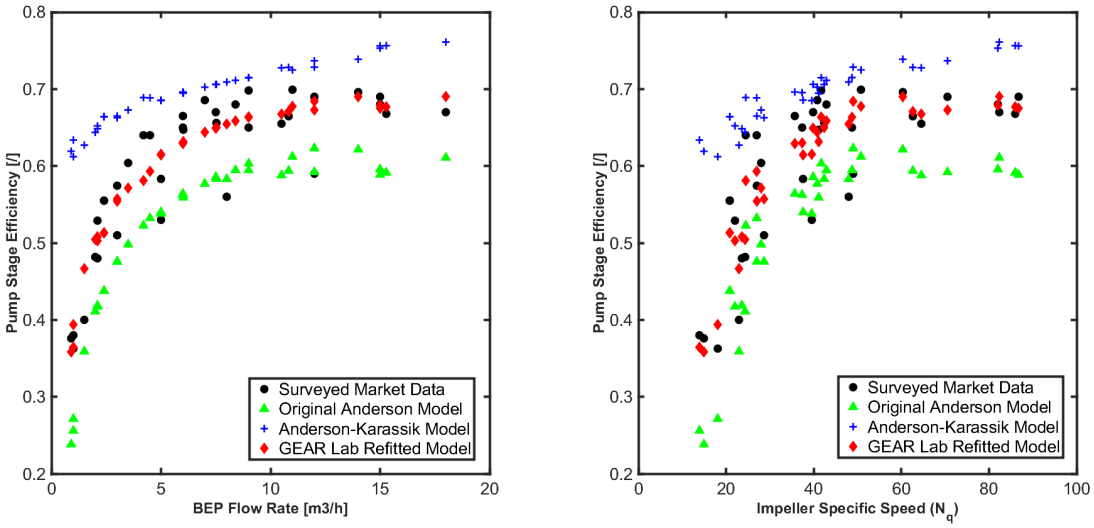

(a) η_{pump}^{MSP} plotted as a function of Q_{BEP} **(b)** η_{pump}^{MSP} plotted as a function of N_q

Fig. 3-1. BEP efficiency prediction models for 4-inch MSP hydraulics plotted as a function of both (a) BEP flow rate and (b) impeller specific speed. Efficiencies of the surveyed market data (black dots), and the predicted efficiencies from the original Anderson model (green triangles), the Anderson-Karassik model (blue crosses), and the refitted GEAR Lab model (red diamonds) are shown. The RMSEs are 14.3891, 19.5488, and 6.4391, respectively.

$$\eta_{pump}^{MSP} = 0.94 - C_1 \cdot \left(\frac{Q(gpm)}{N(rpm)}\right)^{C_2} - 0.29 \cdot \log_{10}\left(\frac{2286}{N_s}\right)^2 \tag{3.4}$$

Table 3.2. Statistically fitted parameters used in Eq. 3.4 for the Anderson-Karassik model [19] and the refitted GEAR Lab model to predict efficiency of 4-inch MSP hydraulic.

Fitted Parameters	Anderson-Karassik	GEAR Lab Model
C_1	0.08955	0.08494
C_2	-0.21333	-0.27246
RMSE	19.5488	6.4391

The trend of the surveyed 4-inch MSP efficiencies in Fig. 3-1 conforms to the qualitative descriptions from the literature [15, 19]. MSPs experience low efficiency at low specific speeds, which translates to the low flow rate region for the 4-inch impellers that have similar H_{st}. The low efficiency is due to the long and radial impeller geometry at low specific speeds. This geometry generates high secondary losses, such as disk friction losses, as well as a high ratio of leakage flow to total flow. As specific speed and flow rate increase,

the impeller design becomes more axial, resulting in a significant reduction of secondary losses. In the same region, the relative leakage flow becomes less significant, contributing to increasing efficiency. This behavior is apparent in the exponential increase of efficiency with specific speed. The efficiency eventually plateaus to a maximum value of approximately 68% for the surveyed 4-inch MSPs.

Since the specific speed is a function of impeller head-per-stage (Eq. 3.1), an empirical relationship is formulated for impeller head-per-stage (in $m/stage$) as a function of BEP flow rate (in m^3/h) for the 4-inch MSP hydraulics. This enables the efficiency prediction for MSPs as a function of Q_{BEP} and H_{BEP} (total head) throughout the hydraulic operating space using Eq. 3.4. The H_{st} for the surveyed 4-inch impeller designs are plotted in Fig. 3-2 as a function of designed BEP flow rate Q. Each of the 37 plotted head-per-stage data are calculated as the linear slope of the total BEP pressure head as a function of the impeller stage quantity, for the 4-inch MSP models that use the same impeller design. A second-order polynomial fit (Eq. 3.5) with an RMSE of 15.284 was imposed to obtain a scaling law for H_{st} as a function of flow rate Q for the 4-inch impellers. As shown in Fig 3-2, the head-per-stage of these impeller designs scatter around an average of 4.32 $m/stage$ but decrease at a higher flow rate. Based on the formulation of Eq. 3.4, the contribution to predicted efficiency from the specific speed term is most sensitive to error in H_{st} when the flow rate is smallest. Although the RSME is relatively high in the modeled H_{st}, the resulting error in the efficiency prediction is < 1.4%, occurring at the minimum flow rate of 1 m^3/h.

$$H_{st} = -0.0120 \cdot Q^2 + 0.1182 \cdot Q + 4.3423 \tag{3.5}$$

3.1.2 Efficiency Prediction for Progressive Cavity Pump Hydraulics

For progressive cavity pumps, previous work has provided theoretical characterizations of PCP performance and designs [37]. More recently researchers have created more sophisticated models to predict the performance of specific PCP designs through CFD, numerical solvers, and 3D-vectoring methods [12, 27, 39]. This work contributes to the theoretical

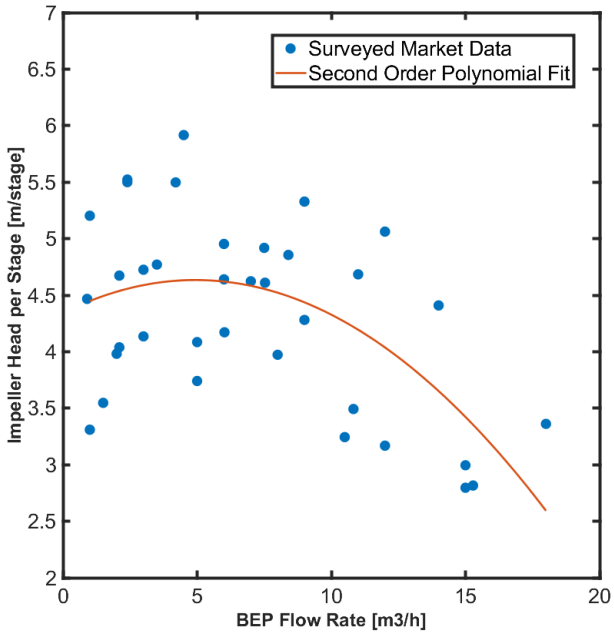

Fig. 3-2. Head-per-stage as a function of BEP flow rate of surveyed impeller designs used in 4-inch MSPs on the market. A second order polynomial fit (Eq. 3.5) is imposed, with a resulting RMSE of 15.284.

understanding of specific PCPs, but it is difficult to generalize beyond the PCP designs used as a basis for each model to explore the full operating space. Since the BEP efficiency of a PCP depends heavily on the fluid viscosity in the application, PCPs were previously designed for moving high viscosity fluids such as petroleum, due to high pump efficiency and low flow slippage in high viscosity operations [25]. However, PCPs are gaining popularity in the smallholder irrigation space and becoming a relatively new technology for low viscosity groundwater pumping applications. This is because of PCPs' high-pressure, low-flow operating space matches the operating requirements of borehole pumping in very smallholder farms. To the author's knowledge, no statistical efficiency prediction model for 4-inch PCPs is found in literature, especially for groundwater-specific applications.

Similar to the MSP case, manufacturer efficiency data of 4-inch borehole PCP hydraulic were surveyed. A third-order logarithmic nonlinear fit was imposed on the surveyed efficiency data and an efficiency scaling law was formulated (Eq. 3.6), resulting in an RMSE value of 5.9247, as shown in Fig. 3-3. Each of the 37 surveyed data points on Fig. 3-3 represents an individual PCP design primarily from Lorentz. This is because PCPs have

not been used in groundwater pumping applications until recently when PVPSs have started to become a cost-effective alternative for very small farms with low flow rate requirements. While PCPs are generally designed to pump fluid with a higher viscosity than water, Lorentz is one of the few manufacturers that have both designed PCPs for borehole applications and documented the pump efficiency testing results [21].

Among the 4-inch PCPs surveyed, the available BEP flow rate range was between 0.3 m^3/h to 3.2 m^3/h, with a BEP pressure head up to 250 m. This operational range defines the Q-H operating space for PCP in the analysis. The hydraulic operating range of PCP covers the low flow rate operating region in the SSA smallholder irrigation space, making them applicable for very smallholder farms (< 1 Ha). In addition, the high end of the PCP operational flow rate range overlaps with the low end of the MSP operational flow rate range, primarily in the Q_{BEP} range between 1 m^3/h and 3.2 m^3/h. In the operating region where both pump hydraulics are applicable, energetic cost comparisons between solar pump hydraulics can be done to identify the most energetically cost-effective pump hydraulic in the architecture. Example comparisons are discussed in Sections 3.3 and 4.2.

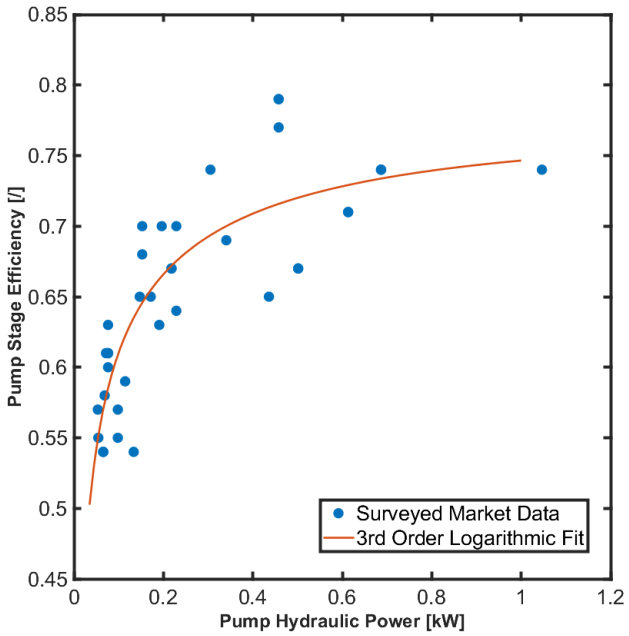

Fig. 3-3. Surveyed efficiencies of 4-inch PCP hydraulic on the current market, primarily from Lorentz, as a function of hydraulic output power. A third-order logarithmic fit (Eq. 3.6) is imposed, with with a resulting RMSE of 5.9247.

$$\eta_{pump}^{PCP} = -0.0689 \cdot \log_{10}(P_{hyd})^2 + 0.0672 \cdot \log_{10}(P_{hyd}) + 0.7465 \tag{3.6}$$

From the surveyed PCP efficiency data, it was found that the BEP efficiency of PCP hydraulics in the 4-inch borehole market scale with the BEP hydraulic power, which is itself the product of the output flow rate and pressure. The efficiency of the pump also scales more significantly with increasing pressure and very slightly with an increase in flow rate. No discernible trend in the efficiency scaling with specific speed was found. The scaling of efficiency with hydraulic power differs from previously reported models which typically present efficiency as a function of only pressure differentials related to specific PCP models [12, 37]. The trend in efficiency scaling can be explained by considering the loss mechanisms in PCPs, which can be characterized by the volumetric losses and mechanical losses previously reported in the literature. Volumetric losses of a PCP are shown to increase with rotor speed and decrease with increasing pressure difference. Mechanical losses due to rotor-stator friction increase with rotor support forces and decrease with increasing pressure difference due to lower friction with higher internal pressure. Since PCPs designed for borehole water pumping generally have an overlapping elastomer coated stator, the mechanical losses significantly dominates over the volumetric losses as discussed by Vetter [37]. The strong increase in BEP efficiency with pressure head can be explained by diminishing and dominant mechanical losses as the pressure differential increases. The slip flow remains approximately constant with pressure differential, resulting in diminishing volumetric losses relative to total flow rate as flow rate increases. This could explain the slight positive correlation between efficiency and the increasing flow rate observed in surveyed data.

3.2 Efficiency Predictions for 4-Inch Submersible Motors

Two types of motors can be used to drive submersible pumps in a PVPS [5]. An AC induction motor (IM), or asynchronous motor, is a traditional solution commonly used in the pump industry to drive submersible pumps due to their simple design, robust mechanism,

and ability to run directly off the AC grid. However, to take advantage of the permanent magnetic fields and the lack of induction losses, the pump industry is slowly transitioning to use submersible permanent magnet brushless DC motors (PM-BLDC) or synchronous motors. This new type of motor allows pump manufacturers to leverage a higher motor efficiency at the same power level compared to the traditional AC solution. When designing for a solar-powered pumping system, the BLDC motors can run directly on the DC power generated from the solar array, without an inverter, which reduces the overall complexity of the electrical system. In addition, BLDC motors can operate below 48 volts, which eliminates the need of building a high voltage solar array or installing a boost converter to meet the voltage requirements of conventional 220V IMs. Most importantly, the higher efficiency of the BLDC motors can lead to a reduction in solar array size and achieve energetic cost savings when compared to the IMs for the same pump body.

To estimate the electrical power via Eq. 2.3, a model of the motor efficiency as a function of shaft power is needed. To the author's knowledge, a scaling law for 4-inch submersible motors' efficiencies has not yet been published. To derive an empirical model, a survey was conducted of 4-inch IMs that are commonly used to drive borehole pumps in a PVPS and which are available in SSA. The surveyed efficiencies of 4-inch IMs are plotted in Fig. 3-4 as a function of shaft power, along with four IE ratings [16]. The IEC 60034-30-1 standard defines four international efficiency classifications for electric motors: IE1, IE2, IE3, and IE4. When an electrical motor sold on the market is certified with a certain IE rating, it has the operating efficiency specified in the IEC standard at the corresponding power level. The data set presented contains 94 AC IMs with an output shaft power ranging from $0.37kW$ up to $7.5kW$. These efficiency data are based on published specifications from four dominant pump manufacturers in SSA: Grundfos, Lowara, Lorentz, and Dayliff [14, 38, 21, 10]. A 4th-order logarithmic nonlinear fit (Eq. 3.7) identical to the interpolation equation presented in the IEC standard is imposed on the collected IM efficiency data as a function of output shaft power. A statistical efficiency prediction law is formulated with a resulting RMSE of 4.7176. The corresponding interpolation coefficients are presented in Table 3.3.

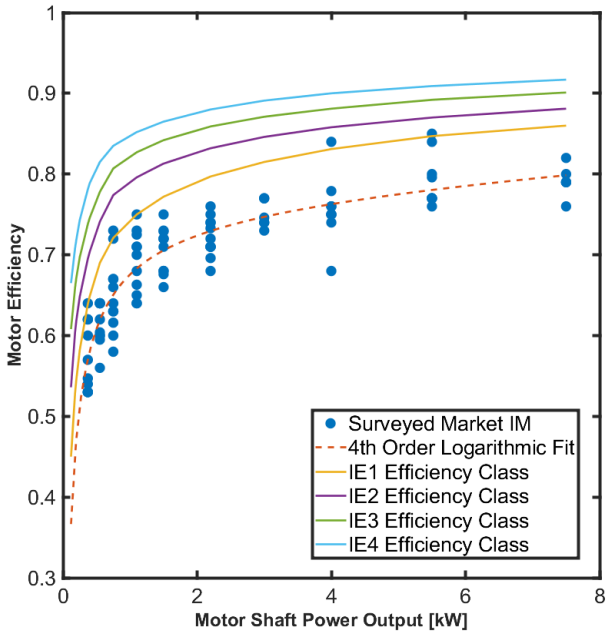

Fig. 3-4. Efficiencies of the surveyed 4-inch IMs and the four IE ratings [16]. A 4-th order logarithmic fit is imposed, with an RMSE of 4.7176. The 4-inch IMs on the market underperform the lowest IE1 efficiency rating.

$$\eta_{motor}(\%) = C_1 \cdot \log_{10}(P_{shaft})^3 + C_2 \cdot \log_{10}(P_{shaft})^2 + C_3 \cdot \log_{10}(P_{shaft}) + C_4 \qquad (3.7)$$

As shown in Fig.3-4, the 4-inch submersible IMs currently sold on the market significantly underperform even the lowest IE1 motor efficiency rating by an average of 0.07 in terms of efficiency. This deficiency in induction motor (IM) efficiency performance suggests a potential opportunity to improve PVPS system efficiency and achieve potential cost savings with higher efficiency motors. In practice, BLDC motors are often found to have comparable or even superior efficiency to the IE3 or IE4 efficiency rating [11]. In the subsequent analysis, the IEC standards will be used to represent potential motors with higher efficiencies that are not yet widely available in the market, such as the BLDC motors. These highly efficient BLDC motors could bring significant efficiency improvement to the existing PVPS and reduce the energetic cost of the solar pump. However, the cost of manufacturing high-efficiency BLDC motors is more expensive than the traditional IMs, because

Table 3.3. Coefficients for efficiency interpolation of the surveyed IMs and the four IE efficiency classes (2-poles, 3000 rpm) [16].

Coefficients	Surveyed IMs	IE1	IE2	IE3	IE4
$0.12kW < P_{shaft} < 0.75kW$					
C_1	6.1369	11.924	22.4864	6.8532	-8.8538
C_2	-10.5895	6.3699	27.7603	6.2006	-20.3352
C_3	18.6090	30.0509	37.8091	25.1317	8.9002
C_4	67.5673	76.6136	82.458	84.0392	85.0641
$0.75kW < P_{shaft} < 7.5kW$					
C_1	6.1369	0.5234	0.2972	0.3569	0.34
C_2	-10.5895	-5.0499	-3.3454	-3.3076	-3.0479
C_3	18.6090	17.4180	13.0651	11.6108	10.293
C_4	67.5673	74.3171	79.077	82.2503	84.8208
Interpolation valid for motor rated power: $0.12kW < P_{shaft} < 7.5kW$.					

BLDC motors often employ rare-earth permanent magnets. To determine the true cost benefits of the highly efficient BLDC motors, solar pump manufacturers can leverage the technoeconomic framework presented in this thesis to quantify the energetic cost-savings of an IE3 or IE4 motor over a traditional IM, at the operating region of interest. The simulated energetic cost savings can be compared to the price difference between a BLDC motor and a traditional IM to identify the most cost-effective motor option in a solar pump architecture.

3.3 Total Efficiency

The efficiency prediction models presented in the previous sections (Sections 3.1 and 3.2) were used to characterize the total efficiency of 10 solar pump architectures, enumerated in Table 3.1. Figure 3-5 presents results for IM-driven MSPs (Fig. 3-5a) and IM-driven PCPs (Fig. 3-5b) to compare the efficiency performance between the two hydraulics. Similar figures for the remaining architectures appear in Appendix C. The x-axes are on different scales due to the difference in operational flow rate range between MSP and PCP hydraulics. An overlapping flow rate range exists between 1 m^3/h and 3.2 m^3/h. By simulating the total efficiency over a range of Q_{BEP} and H_{BEP}, a bird's-eye view of the efficiency performance

can be formulated across the operating space.

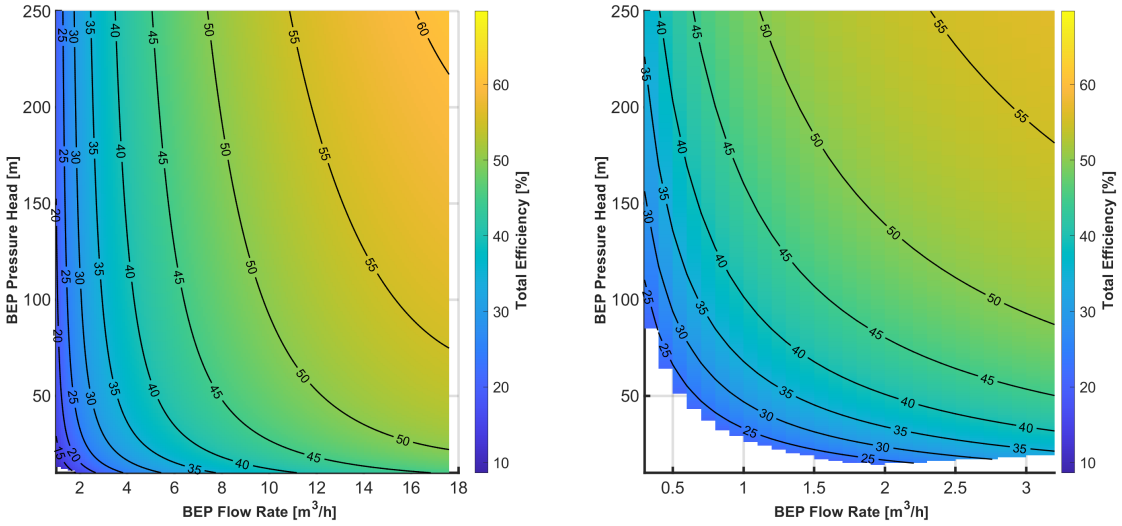

(a) η_{tot} of IM-driven MSPs

(b) η_{tot} of IM-driven PCPs

Fig. 3-5. Total efficiency as a function Q_{BEP} and H_{BEP} of 4-inch borehole pump hydraulics: (a) IM-drive MSPs and (b) IM-driven PCPs. Constant total efficiency contour lines are superimposed. Note the difference in x-axis scaling due to the operating flow rate range difference between the two hydraulics.

As shown in Fig. 3-5a, IM-driven MSPs have total efficiencies of above 30% (and up to 60%) at flow rates greater than 3 m^3/h. However, IM-driven MSPs suffer from sub-30% total efficiencies below 3 m^3/h, where MSP's flow rate range overlaps with PCP's. This is due to the low efficiencies of the impeller in the low flow rate region (Fig. 3-5a) and the induction motor in the low power region (Fig. 3-4). The flow rate range below 3 m^3/h represents the flow rate requirements of the very smallholder farms, typically under 1 Ha. In contrast to the IM-driven MSPs, IM-driven PCPs can generally achieve higher total efficiencies greater than 40% (and up to 55%) in the overlapping flow rate range as shown in Fig. 3-5b. By comparing the total efficiencies of the IM-driven MSP and the IM-driven PCP, it demonstrates that PCP hydraulic is the more efficient and energetically cost-effective solution in the low flow rate operating region. Solar pump manufacturers may want to consider using PCP hydraulic when designing 4-inch solar pumps for the very smallholder market in SSA. On the other hand, PCP hydraulics surveyed are unable to reach a BEP flow rate higher than 3.2 m^3/h, limiting their use for higher flow applications such

as in farms larger than 1 Ha.

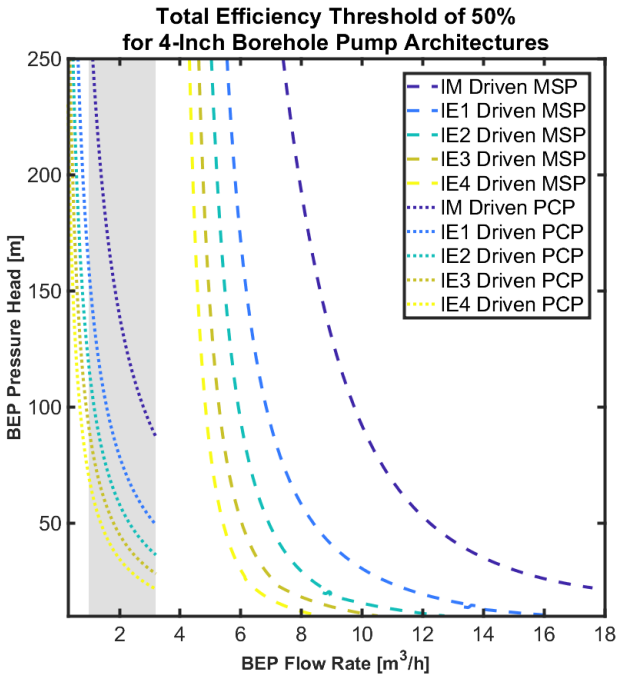

Fig. 3-6. Constant total efficiency isolines of 50% as a function of Q_{BEP} and H_{BEP}, for the 10 solar pump architectures listed in Table 3.1. The shaded region represents the overlapping operating range between the MSP and PCP hydraulics.

By using 50% as a threshold of high total efficiency, Fig. 3-6 superimposes the 50% constant efficiency isolines for all 10 solar pump architectures listed in Table 3.1 in a single plot. This provides a direct comparison and better visualization of the efficiencies for the considered architecture options over the operating space. The operating region to the upper right of the isoline for the corresponding architecture has a total efficiency greater than 50%, and vice versa. The overlapping operating region between the MSP and PCP hydraulics is shaded. The left bound of the shaded region is defined by the minimal Q_{BEP} of MSP at 1 m^3/h, and the right bound is defined by the maximum Q_{BEP} of PCP at 3.2 m^3/h. As shown in Fig. 3-6, 4-inch PCPs are capable of operating in the low flow rate region, while MSPs can operate in a higher and wider flow rate range.

Figure 3-6 highlights operating regions where each solar pump architecture suffers from low total efficiency (< 50%). It demonstrates the benefit of adopting highly efficient BLDC motors (IE3 or IE4 equivalent) to drive MSP and PCP hydraulics in the 4-inch borehole pump operating space. When driven with IMs on the current market, both MSP and PCP

hydraulics are unable to achieve total efficiency above 50% in approximately half of their corresponding operating spaces. In Fig. 3-6, IM-driven MSPs in general can only achieve > 50% total efficiency at $Q_{BEP} > 10\ m^3/h$ and $H_{BEP} > 50\ m$. For IM-driven PCP, the high total efficiency (> 50%) operating region is approximately with Q_{BEP} ranging from $2\ m^3/h$ to $3.2\ m^3/h$, and $H_{BEP} > 100\ m$. Both IM-driven hydraulics experience total efficiency of less than 50% in the remaining operating space, due to the limitation in 4-inch IM efficiency. However, when paired with a BLDC motor that is IE4 efficient, Fig. 3-6 shows total efficiency > 50% can be achieved in operating regions with $Q_{BEP} > 5\ m^3/h$ for MSPs and $Q_{BEP} > 0.8\ m^3/h$ for PCPs, over a wide pressure range. This demonstrates adopting BLDC motors enables an extended reach of the high-efficiency solar pumps in operating regions where total efficiency is currently underperforming due to deficiencies in IMs. By filling in the deficiency gap of IMs, BLDC motors can bring potential cost benefits from high-efficiency solar pumps to a larger group of SSA smallholder farmers, enabling faster adoption of PVPSs to provide reliable water access.

3.4 Volumetric Specific Energy

The volumetric specific energy can be used as a metric to evaluate the sensitivity to energy consumption for per-unit water pumped by a given architecture in various hydraulic operating regions. The volumetric specific energy for each of the 10 solar pump architectures listed in Table 3.1 is calculated using Eq. 2.12 over a range of Q_{BEP} and H_{BEP} within the operating space. The e_{sys} can be related to the energetic cost using Eq. 2.13. When calculating the e_{sys} for a specific solar pump architecture, the empirical efficiency scaling relationships are taken into account. In Fig. 3-7, the volumetric specific energy for IM-driven MSP (Fig. 3-7a) and IM-driven PCP (3-7b) is plotted as a function Q_{BEP} and H_{BEP}. The e_{sys} plots of the remaining architecture options are presented in Appendix D.

By simulating volumetric specific energy across the hydraulic operating space, it highlights regions where per-unit-cost of water is most energetically expensive and efficiency improvements can be most pronounced for a given solar pump architecture. As shown in Fig. 3-7, high e_{sys} is observed in the high-pressure, low flow rate hydraulic operating

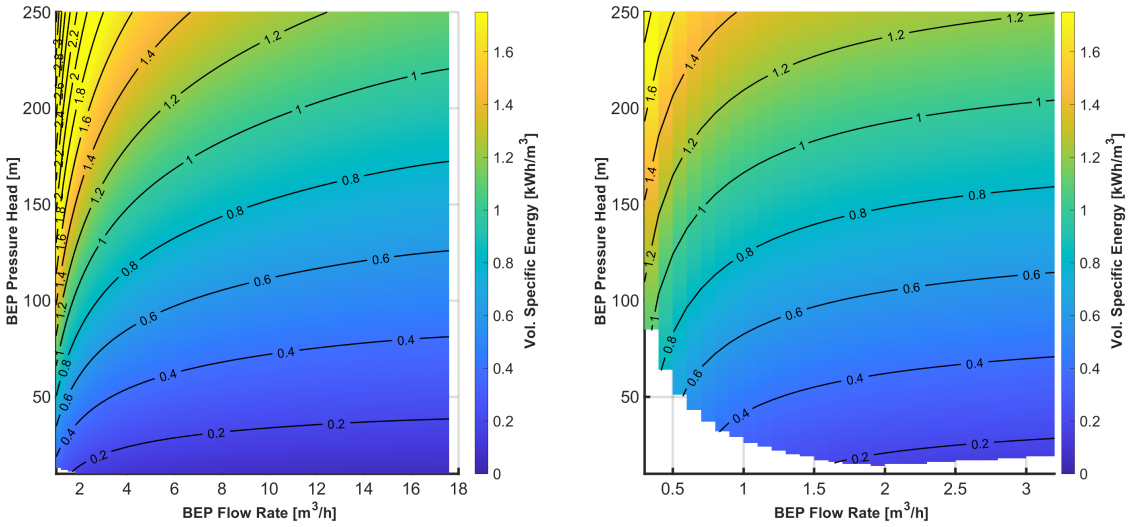

(a) e_{sys} of IM-driven MSPs

(b) e_{sys} of IM-driven PCPs

Fig. 3-7. Volumetric specific energy as a function of Q_{BEP} and H_{BEP} for (a) IM-driven MSPs and (b) IM-driven PCPs. Note the difference in x-axis scaling due to the operating flow rate range difference between the two hydraulics.

regions correspond to MSP and PCP hydraulics. This represents the per-unit energetic cost of water is more expensive when a solar pump is operating in a high-pressure, low flow rate environment. This is likely due to two synergistic factors. First, both the pump hydraulic and motor experience a low efficiency in the low flow rate, low-power region, resulting in poor total efficiency for the solar pump (Fig. 3-5). Second, the electrical power required to produce a high-pressure head is high. As a result, the amount of electrical energy needed to move a cubic meter of water, represented by the e_{sys}, is significantly higher in the high-pressure, low-flow rate region. This identifies a potential opportunity for solar pump manufacturers: using highly efficient BLDC motors for high-pressure, low flow rate applications, such as a small farm with a deep borewell, can effectively reduce the per-unit cost of water in a solar-powered pumping system.

By simulating the η_{tot} and e_{sys} over the operating space, solar pump manufacturers can use the reference plots produced by the efficiency prediction models to visually examine the technical performance of different solar pump architectures. The models enable them to identify operating regions that experience shortcomings in solar pump efficiency and understand the potential impacts of efficiency improvement strategies, such as using a

BLDC motor. By adopting highly efficient BLDC motors, it allows 4-inch solar pumps to effectively extend the reach of high efficiency operating regions and reduce the per-unit energy cost of water.

Chapter 4

Example Case Studies: Applications to SSA Farms

In this chapter, the technoeconomic framework was used in combination with the efficiency prediction models formulated for the 4-inch borehole pump architectures to conduct case study analyses on SSA farms. Two types of analyses are presented to demonstrate the application of the framework in characterizing the energetic costs attributable to the efficiency performance of the different solar pump architectures in specified operating conditions.

First, the operating space-level analysis quantifies and compares the energetic costs between two solar pump architectures over the operating space. This type of analysis provides a bird's-eye view of the potential energetic cost-savings generated from efficiency improvement of the relatively more efficient solar pump architecture out of the two compared options in different hydraulic operating regions. The second analysis presents a similar energetic cost quantification for all considered solar pump architectures about a specific operating point. The goal of this analysis is to identify the most energetically cost-effective solar pump architecture when designing PVPS based on a set of specific requirements from an end-user.

For both case studies discussed in this chapter, the operating location is set in Nairobi, Kenya, which has a very active solar irrigation market. The t_{irr} is chosen to be the typical 6 hours based on interviews with SSA farmers who have a PVPS. The location-specific PV output potential PV_{out} is 4.1918 kWh/kW_p based on modeled solar GIS data [36].

The retail price of the solar panels is 810 USD/kW_p reported locally [8]. These input parameters are listed in Table 4.1.

Table 4.1. Input parameters used for the example case studies in SSA.

Input Parameters	Values
Location	Nairobi, Kenya
Latitude	-1.2921
Longitude	36.8219
PV_{out} (GSA)	4.1918 kWh/kW_p
t_{irr}	6 hours
C_{sol}	\$0.81 USD/kW_p

4.1 Operating Space-Level Comparative Analysis

Two solar pump architectures were compared in this operating space-level case study: IM-driven MSP and IE4-driven MSP. The purpose of this example case study is to quantify the amount of energetic cost-savings that a solar-powered MSP would have when an IE4 efficient BLDC motor is used over a traditional IM, in the various operating regions. In Fig. 4-1, the energetic costs of IM-driven MSPs (Fig. 4-1a) and IE4-driven MSPs (Fig. 4-1b) are plotted as a function of Q_{BEP} and H_{BEP}. The results were calculated using Eq. 2.5, based on the hydraulic operating points, predicted efficiencies of the hardware, and the input parameters listed in Table 4.1.

As shown by both plots in Fig. 4-1, the costs of the solar array scale predominantly with the hydraulic operating power. The energetic cost is highest in the high flow rate, high-pressure region for both solar pump architectures. The energetic cost of the IE4-driven MSPs (Fig. 4-1b), which is more efficient, is lower than the IM-driven MSPs (Fig. 4-1a) throughout the operating space. The spacing between the superimposed isolines is wider in the low hydraulic power region because total efficiency increases rapidly in the low flow rate and pressure region of the operating space (Fig. 3-5a). While the hydraulic power scales quadratically as the product of flow rate and pressure, the total efficiency of the solar pump also increases exponentially, compensating for the additional power draw with the reducing

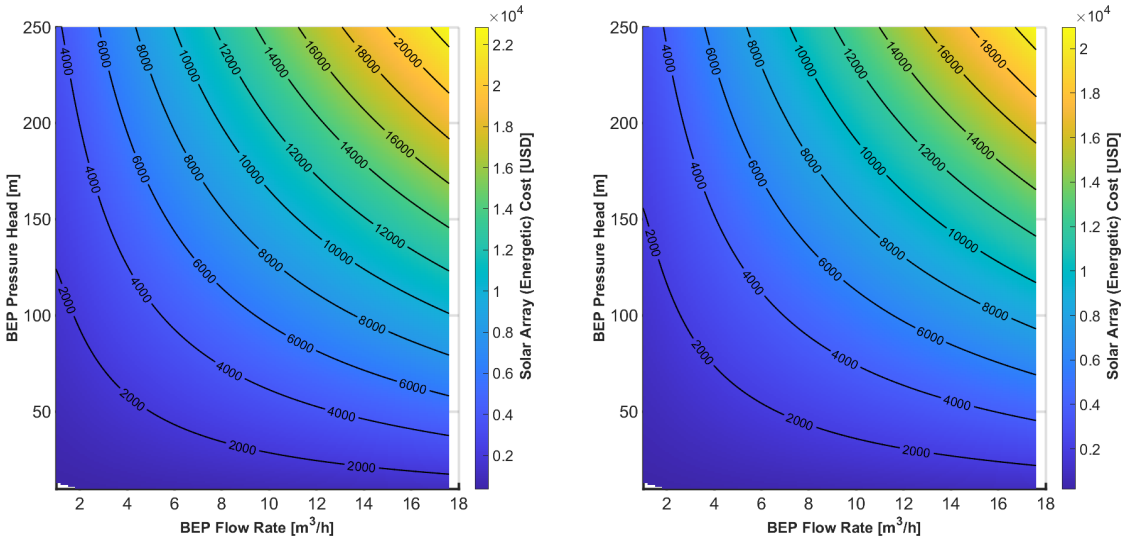

(a) C_{array}^{tot} of IM-driven MSPs

(b) C_{array}^{tot} of IE4-driven MSPs

Fig. 4-1. Solar array (energetic) costs of (a) IM-driven MSPs and (b) IE4-driven MSPs for 6 hour run-time in Nairobi.

power losses in the hardware. This generates a parametric design insight when designing PVPSs in the low flow rate and pressure region. In this region, efforts to reduce PVPS cost by lowering the power draw of the downstream component, such as optimizing the area of the irrigated subsection, would have minimal impact on the energetic cost of a solar pump.

The energetic cost of the IM-driven MSPs in Fig. 4-1a can be broken down into the hydraulic power contribution (Eq. 2.8), and the inefficiency contributions from the pump hydraulic (Eq. 2.9) and the motor (Eq. 2.10). In Fig. 4-2a, the total energetic cost and the respective cost contributions are plotted as a function of flow rate and pressure. To provide a more granular understanding of the dominating cost driver, a pressure cut-plane of 25 m is selected based on the common water table depth across SSA [23]. The cross section of Fig. 4-2a at pressure head of 25 m is plotted in Fig. 4-2b, where the corresponding costs are presented as only a function of flow rate.

As shown in Fig. 4-2b, the dominant energetic cost driver of a solar pump changes at the different power levels. For the IM-driven MSPs at a 25 m pressure head, the dominant energetic cost driver is the necessary hydraulic power for the majority of the high power operating range above 3 m^3/h flow rate. However, for flow rates < 3 m^3/h, the primary

energetic cost contribution becomes the inefficiency of the solar pump. While the < 3 m^3/h flow rate range represents the smallholder farmers with < 1 Ha of irrigated land, it demonstrates that the majority of the energetic cost paid by these farmers for an IM-driven MSP is to compensate for the solar pump inefficiency.

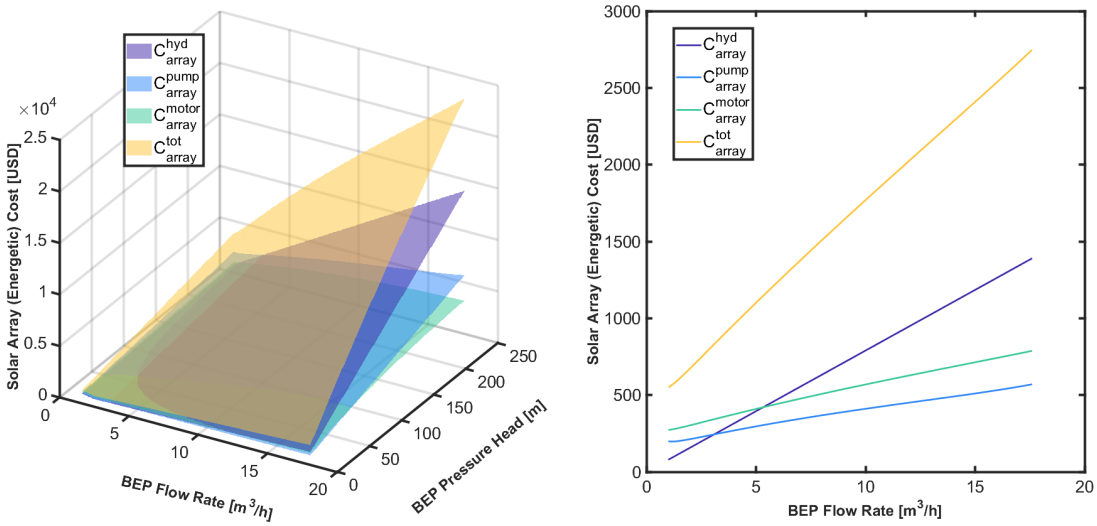

(a) Energetic cost contributions in 3D **(b)** Energetic cost contributions along $H = 25\ m$

Fig. 4-2. (a) Energetic cost contributions plotted in 3D and (b) energetic cost contributions along a constant pressure cross section of 25 m for IM-driven MSPs in Nairobi with 6 hours of system run time. The total energetic cost (paige) consisted of three contributions: hydraulic power (purple), and inefficiency from the pump hydraulic (blue) and motor (green).

The difference in the energetic costs between the IM-driven MSPs (Fig. 4-1a) and the IE4-driven MSPs (Fig. 4-1b) can be calculated using Eq. 2.6. The result is plotted in Fig. 4-3a and it represents the energetic cost-savings (USD) that an IE4 motor has over traditional IM when driving a MSP hydraulic. The percentage energetic cost-savings is also calculated using Eq. 2.7 and plotted in Fig. 4-3b.

Based on the simulated results shown in Fig. 4-3a, the energetic cost-savings scale primarily with the solar pump hydraulic power. The largest cost savings are observed in the high hydraulic power region. At high hydraulic power, the higher IE4 motor efficiency makes a larger impact on the required electrical power and size of the solar array. As a result, there is a big economic incentive for solar pump manufacturers to provide higher efficiency motor in the high power region, as the energetic cost-savings are likely to outweigh

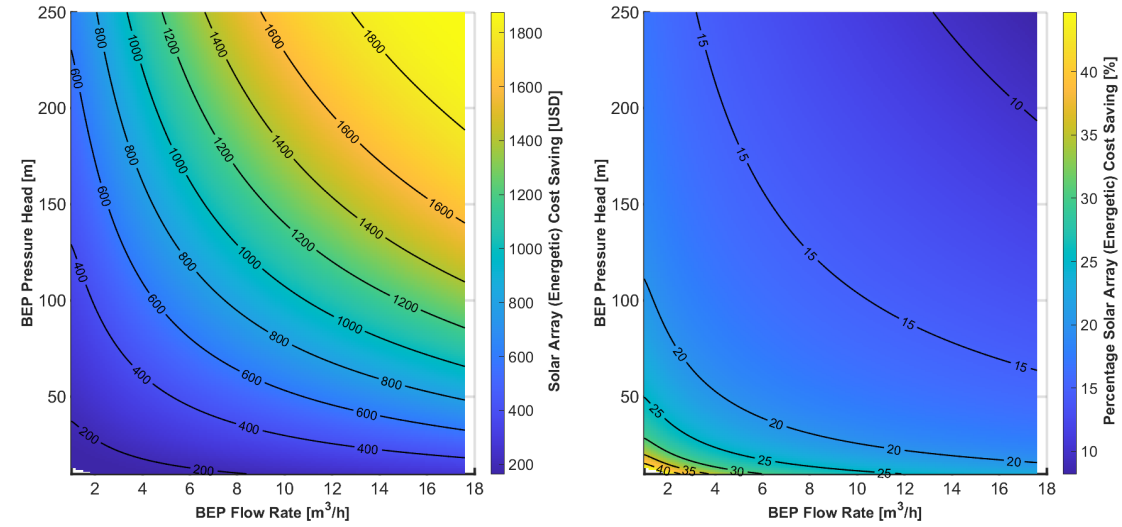

(a) Solar array (energetic) cost-savings **(b)** Percentage energetic cost-savings

Fig. 4-3. (a) The energetic cost-savings in USD and (b) the percentage energetic cost-savings in % comparing IM-driven MSPs to IE4-driven MSPs as a function Q_{BEP} and H_{BEP}. The operating conditions are listed in Table 4.1.

the additional capital cost of the more efficient motor. In addition, Fig. 4-3a provides a guideline on the capital cost premium that a more efficient motor can have before the cost benefits from the efficiency gain break even.

However, Fig. 4-3b shows the largest percentage of cost-savings occurs at the low hydraulic power region. In the low hydraulic power region, the efficiency difference between an IE4 motor and an IM is larger, and the energetic cost associated with the power losses in the hardware is also more prominent. Therefore, although there is not a large energetic cost-saving, the economic impact of efficiency gain is most pronounced in the low power region. It demonstrates the potential needs for low-cost, high-efficiency motors for PVPS in the low power region, which represents the operating space of the very smallholders, who are more likely to be in poverty.

By quantifying the energetic costs over the operating space, the framework allows direct evaluation of the potential energetic cost-savings when comparing two solar pump architectures. Solar pump manufacturers can repeat this analysis for the different architecture options and relate efficiency performance to the capital cost of the solar array to form a baseline of direct cost comparison. By comparing the energetic cost-savings to the capital

cost difference, this analysis enables manufacturers to make informed technoeconomic decisions when designing solar pumps that are more cost-effective in the various operating regions.

4.2 Operating Point-Level Comparative Analysis

In this section, the energetic cost analysis was conducted for a specific hydraulic operating point. This enables direct energetic cost comparison between all considered solar pump architectures when designing a PVPS for a set of specific operating requirements - which could come from the end-user. In this case study, the operating point with Q_{BEP} of 3 m^3/h and a H_{BEP} of 25 m is considered, and the operating conditions listed in Table 4.1 are used. The selected operating point represents the approximate operating requirements of a 1 Ha smallholder farm with a 25 m deep borehole. All 10 solar pump architectures listed in Table 3.1 were found to be viable for this operating point. The energetic cost of each solar pump architecture is calculated and plotted in Fig. 4-4 in terms of cost contributions.

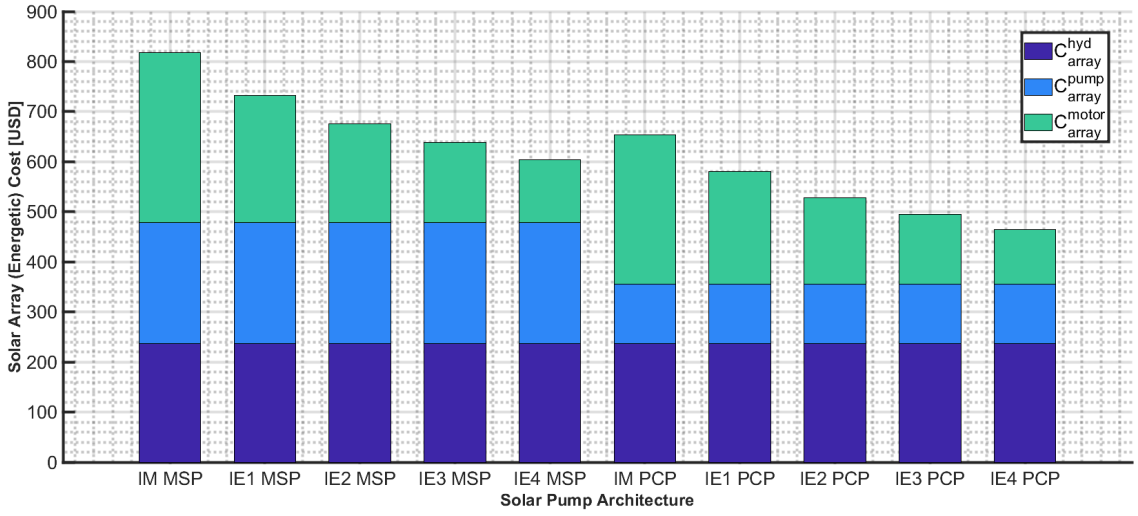

Fig. 4-4. Stacked plot of the solar array (energetic) cost contributions of the 10 viable solar pump architectures (Table 3.1) for Q_{BEP} = 3 m^3/h, H_{BEP} = 25 m, and the operating conditions listed in Table 4.1. The energetic cost is broken down to three contributions: hydraulic power (purple), inefficiency of the pump hydraulic (blue) and motor (green).

The simulated results show that the PCP hydraulic efficiency outperforms MSP at this

operating point. However, the efficiency deficiency of the MSP can be compensated with a more efficient IE4 motor to become more energetically cost-effective than an IM-driven PCP. The exact values of the simulated array power and associated costs are tabulated in Appendix E. A system designer may use these quantified energetic costs and compare them with hardware procurement cost information to make an informed decision on the most cost-effective architecture. If the capital cost of a PCP does not exceed the difference in the energetic cost in the solar array compared to the less efficient MSP hydraulic, then the designer may choose a PCP as the hydraulic in the solar pump architecture, and vice versa. Similarly, the system designer may also consider the potential motor options and decide if the additional upfront cost of a more efficient submersible motor outweighs its energetic cost benefits to a less efficient motor. This energetic cost quantification from the solar pump architecture design perspective can allow system designers to conduct trade-off analyses and select the most cost-effective solution for the needs of the local farmers.

Chapter 5

Discussion

To reduce the high PVPSs upfront cost which poses a financial burden for SSA smallholder farmers, a study was put forth to investigate the cost-saving strategy of improving efficiency from a solar pump architecture perspective. While solar pumps are the largest energy consumers in PVPSs, improving their efficiency can effectively make PVPSs more affordable. A technoeconomic framework is presented to provide a pathway for characterizing the energetic cost implications that arise from the efficiency performance of a solar pump. The framework relates efficiency to the solar array cost, a capital cost, and enables direct comparison to the capital cost of the hardware used in different solar pump architectures. Industrial practitioners can use this framework to compare the potential energetic cost-savings to the capital cost premiums of the more efficient hardware components, identifying the most cost-effective solar pump architecture.

While SSA smallholder irrigation space is used as an example application of the framework, the efficiencies of the commonly used 4-inch borehole pump components are characterized as part of this study. It was found that PCPs outperform MSPs in efficiency over the overlapping hydraulic operating flow rate range of $< 3\ m^3/h$, which corresponds to the flow rate requirement of the $< 1\ Ha$ very smallholder farms. This difference in efficiency performance between the two 4-inch borehole pump hydraulics is visually apparent in the total efficiency plots and the operating point-level case study presented. However, although the framework results have shown PCPs are the more energetically cost-effective pump hydraulic option for solar pump architectures used in very smallholder farms, their overall

cost-effectiveness remains uncertain. Due to the complex helical rotor design used in PCPs, they are generally more expensive and harder to maintain when compared to the simple impeller design used in MSPs. Manufacturers may want to weigh the additional capital cost and maintenance cost of a PCP against its energetic cost benefits over an MSP, which is characterized by the framework, when determining the optimal pump hydraulic used in the architecture. In addition, 4-inch MSPs can reach a higher and wider flow rate range than PCPs, up to $18 m^3/h$ based on the surveyed data, which makes them the sole solution for borehole pumping in medium-scale smallholder farms > 1 Ha.

The efficiencies of the submersible IMs commonly used to drive 4-inch borehole pumps are also surveyed. It was found that the 4-inch IMs currently on the market significantly underperform the lowest international motor efficiency rating, IE1, by an average of 0.07. This implies that the traditional IMs used in the majority of the borehole pumps on the market are not optimal for solar-powered applications. The use of highly efficient BLDC motors (generally IE3 or IE4 efficient) can bring large efficiency improvement and energetic cost-savings to solar pumps. This hypothesis is confirmed by the framework's simulated results presented in this thesis. Based on the total efficiency plots, IM-driven hydraulics are unable to achieve > 50% total efficiency in half of their corresponding operating space. By adopting IE4 efficient BLDC motors, solar pump operating space with > 50% total efficiency is effectively extended, enabling more affordable PVPSs to a majority of SSA smallholder farmers. In addition, by comparing IE4-driven MSPs to IM-driven MSPs in an operating space-level case study, it was suggested the largest energetic cost-saving of > 1800 USD can be achieved in the high pressure, high flow rate region. This demonstrates the potential use of highly efficient BLDC motors in solar pumps can be economically incentivized for manufacturers. This economic incentive is more prominent in the high hydraulic power operating region, where the larger energetic cost-savings are likely to outweigh the capital cost premiums of the more efficient BLDC motors. Moreover, the simulated results have shown that the highest percentage cost savings of up to 40% is in the low hydraulic power region, which represents the very smallholder farms. This demonstrates the potential needs for low-cost, high-efficiency BLDC motors for the very smallholder market in SSA.

The case studies presented in this thesis demonstrate the example use of the frame-

work and the hardware efficiency characterizations to analyze the efficiency performance and derive technoeconomic insights for achieving energetic cost-savings in a solar pump architecture. In this case, the cost-saving strategy was to replace currently inefficient IMs with highly efficient BLDC motors in hydraulic operating regions where the energetic cost-savings outweigh the capital cost premiums. Manufacturers can use this framework and repeat the analytical process to quantify the energetic costs of other solar pump architectures and identify additional cost-saving strategies on PVPSs. Since only the efficiency of 4-inch borehole pump components is characterized, the efficiency prediction models presented may not be valid for other pump types. Manufacturers and researchers can use a similar efficiency characterization process to survey pump types of interest, formulate efficiency prediction models, and utilize the presented framework in quantifying the energetic costs for other solar pumping applications (e.g. desalination, wastewater, and drinking water supply).

Although SSA was used as an example location in this study, the energetic cost framework can also be applied elsewhere. The location-specific parameters used in the framework analysis such as the PV output potential can be adjusted according to the local operating conditions. Also, the solar panel price can be modified to more accurately reflect the price in the various local markets and the potential price changes in the future. With the trend of decreasing solar panel price over time, the affordability of a PVPS may become less sensitive to the solar pump inefficiency, because the cost associated with the additional solar array compensating for the power losses may become less expensive. Since off-grid, solar-powered pumping systems are the focus of this study, the framework defines the energetic cost as the total cost of the solar array. When considering potential grid-tied, hybrid systems, the electricity cost over the systems' operating lifetime can be aggregated and added to the capital cost of the solar array, redefining the energetic cost in the framework. A similar efficiency-related energetic cost comparison to the capital cost of the hardware can then be conducted for grid-tied pumping systems using the modified framework.

When formulating the presented framework, several assumptions were made and some limitations resided. The solar array required to support a specific solar pump architecture is sized using conservation of electrical energy generated from the solar array daily. This

assumes the energy generated can be stored in a sufficiently large energy buffer such as a tank or batteries. By doing so, the average daily PV output potential can be used and the variation in daily solar irradiance can be neglected, reducing computational complexity. However, losses can occur during energy transfer in physical systems from pipe loss and electrical resistance. These losses are expected to be minor when compared to the dominant power losses in the solar pumps. The costs of the power electronics and batteries are also not captured in the scope of this framework since they are largely depend on the physical setup of the actual PVPS. However, PVPS designers may want to consider the costs of the power system components when designing PVPSs at different power ratings.

Moreover, the efficiencies of the solar pump are modeled continuously as a function of the BEP flow rate and pressure. In reality, manufacturers produced pump designs at discrete BEPs (e.g. 1 m^3/h, 3 m^3/h, etc.) with overlapping operating ranges. PVPSs designers may not be able to find solar pumps with specific BEPs that match their desired operating points exactly. This may cause the actual operating efficiency to deviate slightly from the model approximation, but the deviation is likely small when compared to the total efficiency of the solar pump. On the other hand, the energetic costs calculated based on the efficiency models are generalized approximations of the hardware, and these results do not represent the efficiency performance of any specific manufacturer. This is because the efficiency data from multiple manufacturers are lumped together to formulate the efficiency prediction models to represent the general market. In addition, the efficiency prediction model presented for PCP hydraulic is generated based on a relatively small set of commercially available products. As more PCPs are developed for the 4-inch borehole market, the model should be updated with additional efficiency data to further increase its robustness.

Chapter 6

Conclusions

When designing technological solutions for solar-powered applications in developing markets, it is key to understand the energetic cost implications of the system components to provide an affordable solution to extremely cost-sensitive users. In this thesis, a technoeconomic framework is presented to quantify the potential energetic cost-savings that arise from efficiency improvement when comparing solar pump architectures. The SSA smallholder irrigation space is chosen as an example application of this energetic cost framework. The efficiencies of the commonly used 4-inch borehole pump components in the SSA irrigation space were characterized. New efficiency prediction laws were formulated for 4-inch borehole multistage centrifugal pump and progressive cavity pump hydraulics, and submersible induction motors. The IE motor efficiency ratings were used to represent motors with higher efficiencies, such as a brushless DC motor. The solar pump components were put in various configurations to construct different solar pump architectures which are analyzed using the framework in the presented case studies.

Two case studies for SSA farms were simulated to demonstrate the application of the framework in quantifying the energetic costs for different solar pump architectures. For the operating space-level case study, energetic cost-savings were quantified over the multistage centrifugal pump hydraulic operating space when IE4 efficient motors were used over the traditional induction motors on the market. This case study maps out the quantifiable economic incentive for solar pump manufacturers to adopt more efficient BLDC motors in the different hydraulic operating regions. For the operating point-level case study, the

energetic costs of 10 solar pump architectures are simulated for the operating conditions of a 1 Ha SSA smallholder farm with a 25 m borewell. It demonstrates how PVPS designers can use the framework to identify the most energetically cost-effective solar pump architecture for the needs of an end-user.

Some technoeconomic insights were also drawn throughout the thesis when applying the energetic cost framework to the 4-inch borehole pumps used in SSA solar irrigation space. The shortcoming in the efficiency of the induction motors commonly used to drive 4-inch borehole pumps on the market was found. By adopting highly efficient BLDC motors, a considerable amount of efficiency improvement can be achieved and energetic cost-savings can be realized in a solar-powered pumping system. The economic incentive of adopting BLDC motors is most pronounced in the high hydraulic power region. The reduction in per-unit cost of water is greatest in the high pressure, low flow rate region. The largest percentage of energetic cost-savings is in the low power region. It was also found that BLDC motors can effectively extend the reach of high-efficiency solar pumps in the operating space, enabling more energetically cost-effective PVPSs to serve a larger population of smallholder farmers in SSA.

By relating efficiency performance to a quantifiable energetic cost, the presented framework enables industrial practitioners to directly compare the potential energetic cost savings to the capital cost differences in the hardware components of varying efficiencies. Solar pump manufacturers should consider a swift adoption of BLDC motors for driving pumps designed for solar-powered applications. In the process of adoption, the energetic cost-savings that arise from the efficiency gain of the BLDC motors should be weighed against the additional capital cost premiums compared to the traditional IMs, in the various hydraulic operating regions. By incorporating the framework in their design process, it allows industrial practitioners to make informed trade-off decisions when choosing the optimal solar pump architecture. The ability to identify the optimal solar pump architecture allows industrial practitioners to increase the efficiency of current solar pump designs, lower the overall upfront cost of PVPSs, and engage a wider market space with more cost-effective solutions. By providing various technoeconomic insights over the hydraulic operating space from a solar pump architecture perspective, industrial practitioners may find this

framework valuable when designing more affordable, better-performance solar pumps for the developing markets.

Appendix A

Nomenclature

The following symbols are used in this thesis:

C_{array}^{hyd}	=	Cost of solar array due to hydraulic power (USD);
C_{array}^{pump}	=	Cost of solar array due to pump hydraulic body inefficiency (USD);
C_{array}^{motor}	=	Cost of solar array due to motor inefficiency (USD);
C_{array}^{tot}	=	Total cost solar of array (USD);
C_{sol}	=	Retail price of solar panels (USD/kW_p);
E_{elect}	=	Electrical energy (kWh);
e_{sys}	=	Volumetric specific energy (kWh/m^3);
η_{pump}	=	Pump hydraulic body efficiency (/);
η_{pump}^{MSP}	=	Predicted efficiency of MSP hydraulic (/);
$\eta_{pump}^{Anderson}$	=	Predicted efficiency of MSP hydraulic using original Anderson model (/);
η_{pump}^{A-K}	=	Predicted efficiency of MSP hydraulic using Anderson-Karassik model (/);
η_{pump}^{PCP}	=	Predicted efficiency of PCP hydraulic (/);
η_{motor}	=	Motor efficiency (/);
η_{tot}	=	Total efficiency (/);
H	=	Pressure head (m);
H_{BEP}	=	Pressure head at BEP (m);
N_q	=	European specific speed ($rpm \cdot m^{3/4} \cdot s^{-1/2}$);
N_s	=	Imperial specific speed ($rpm \cdot gal^{1/2} \cdot min^{-1/2} \cdot ft^{3/4}$);

N = Pump rotor speed (rpm);

P_{array}^{hyd} = Power of solar array due to hydraulic power (kW_p);

P_{array}^{pump} = Power of solar array due to pump hydraulic body inefficiency (kW_p);

P_{array}^{motor} = Power of solar array due to motor inefficiency (kW_p);

P_{array}^{tot} = Total power of solar array (kW_p);

P_{hyd} = Hydraulic power (kW);

P_{shaft} = Shaft power (kW);

P_{elect} = Electrical power (kW);

PV_{out} = Photovoltaic output potential (kWh/kW_p);

Q = Flow rate (m^3/h);

Q_{BEP} = Flow rate at BEP (m^3/h);

t_{irr} = Time of irrigation (h);

V_{crop} = Crop water demand (m^3);

Appendix B

Solar GIS Map of the Modeled PV_{out} in SSA

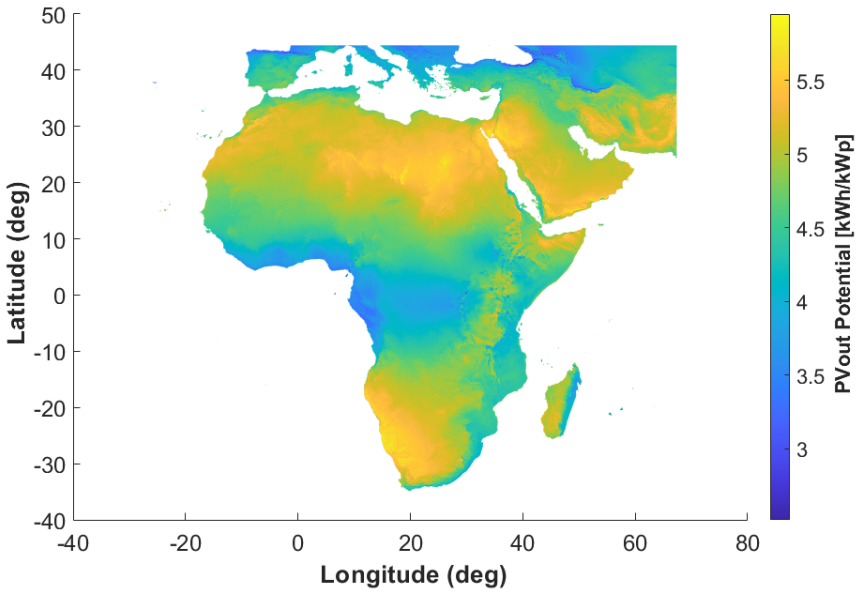

Fig. B-1. Average daily photovoltaic output potential PV_{out} in kWh/kW_p for Sub-Saharan Africa, reproduced from Global Solar Atlas.

Appendix C

Total Efficiencies of Solar Pump Architectures Listed in Table 3.1

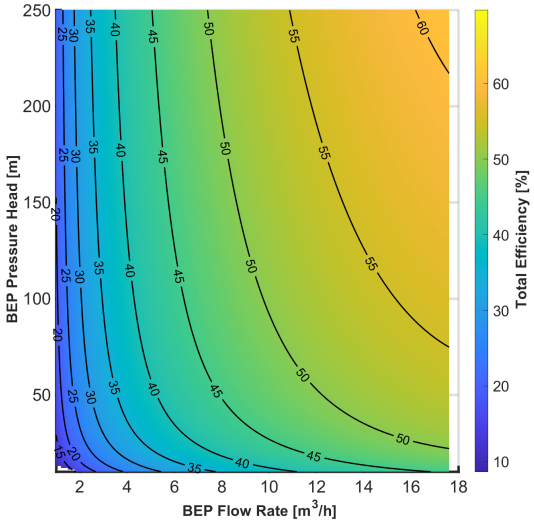

(a) IM-Driven MSP

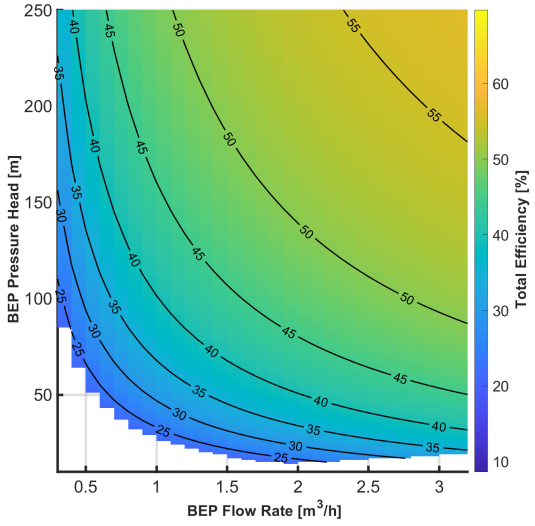

(b) IM-Driven PCP

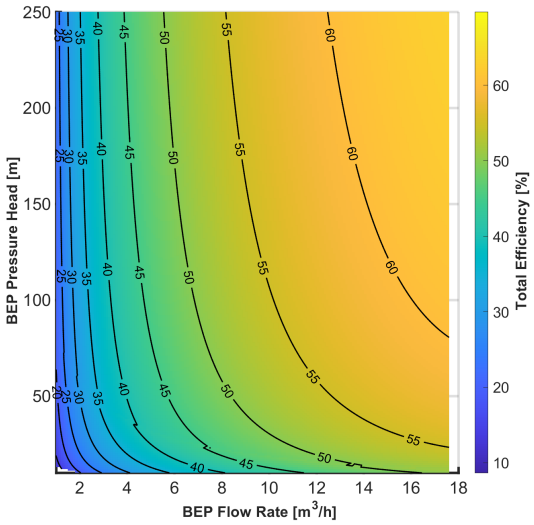

(c) IE1-Driven MSP

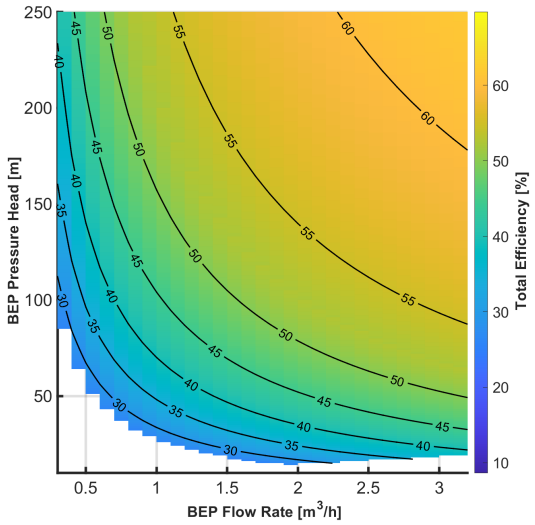

(d) IE1-Driven PCP

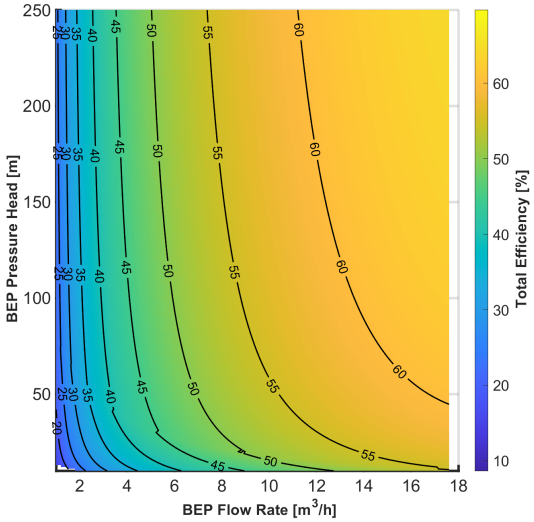

(e) IE2-Driven MSP

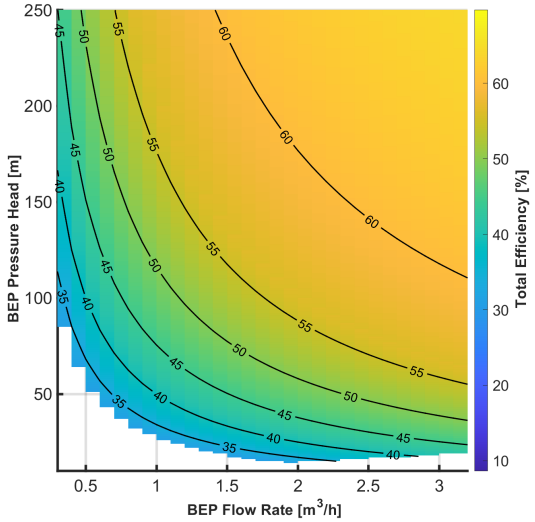

(f) IE2-Driven PCP

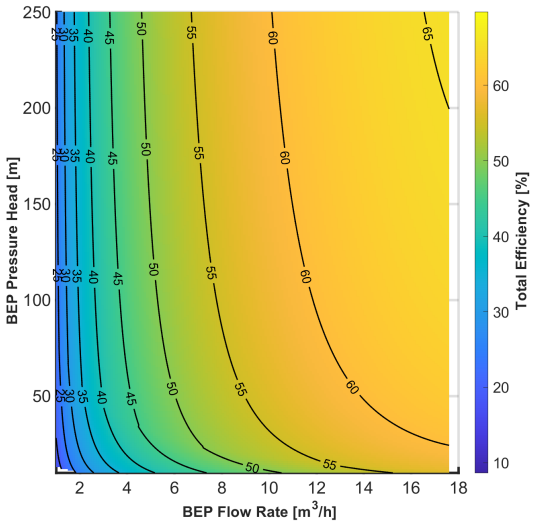

(g) IE3-Driven MSP

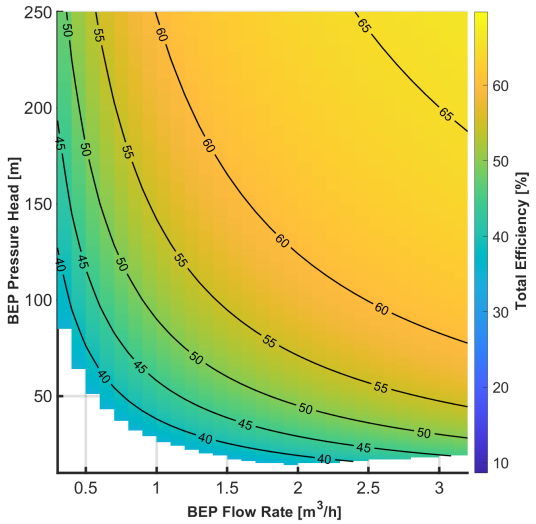

(h) IE3-Driven PCP

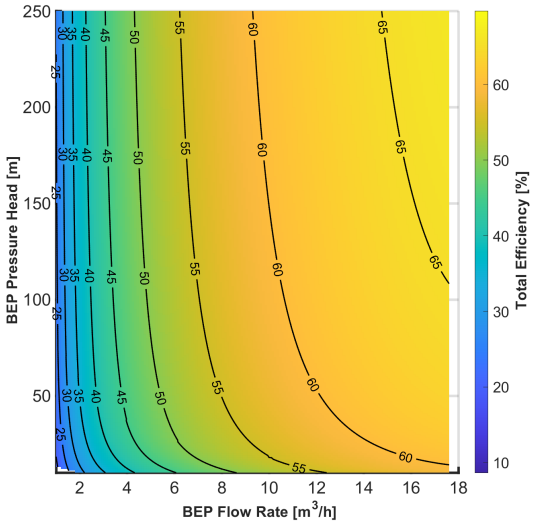

(i) IE4-Driven MSP

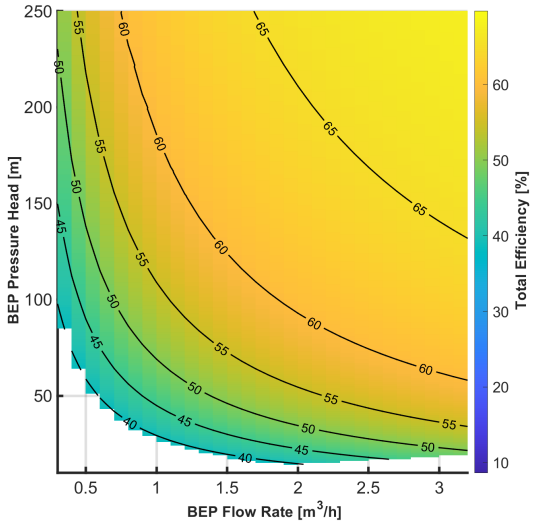

(j) IE4-Driven PCP

Fig. C-1. Total efficiency plots for all listed solar pump architectures listed in Table 3.1, as a function of Q_{BEP} and H_{BEP}.

Appendix D

Volumetric Specific Energy of Solar Pump Architectures Listed in Table 3.1

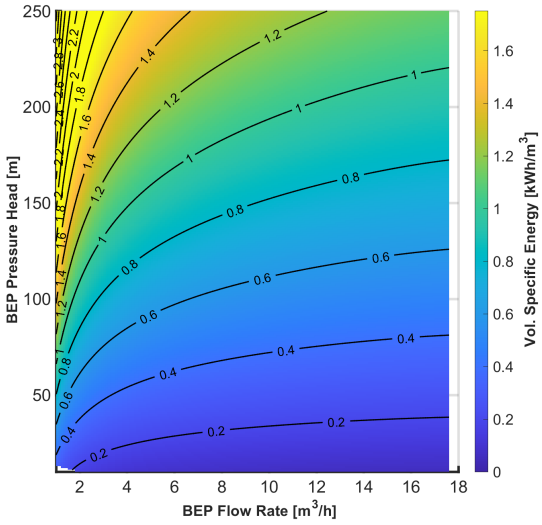

(a) IM-Driven MSP

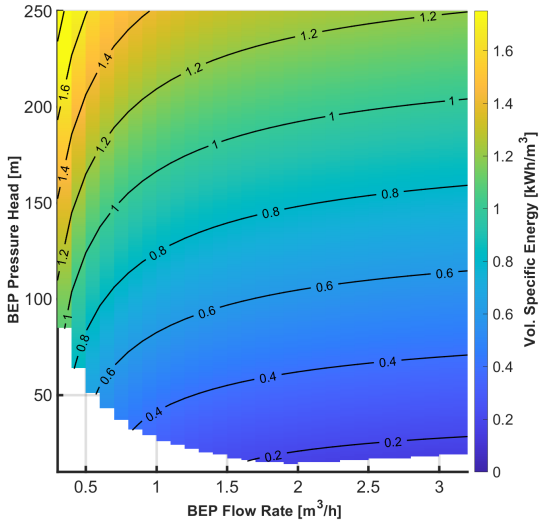

(b) IM-Driven PCP

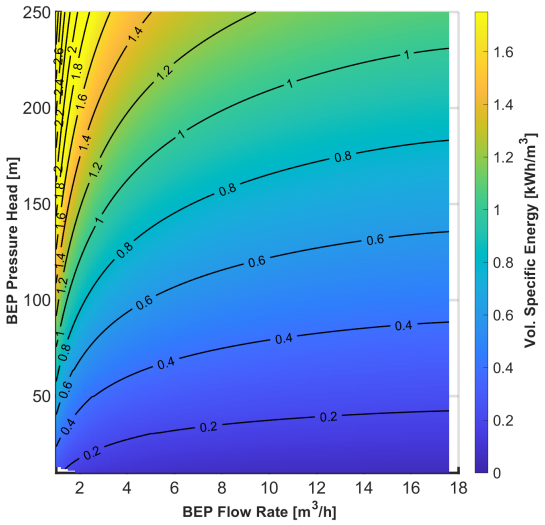

(c) IE1-Driven MSP

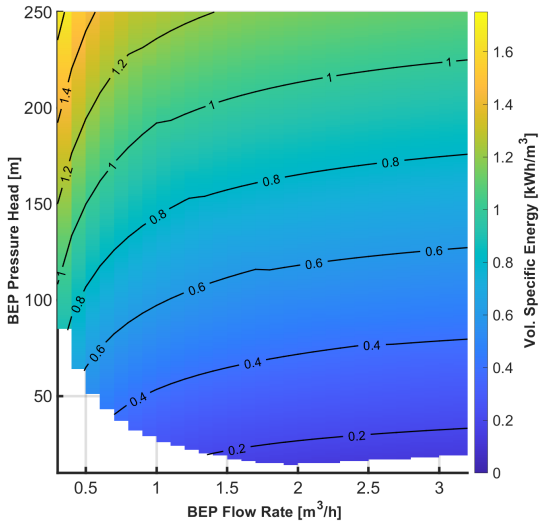

(d) IE1-Driven PCP

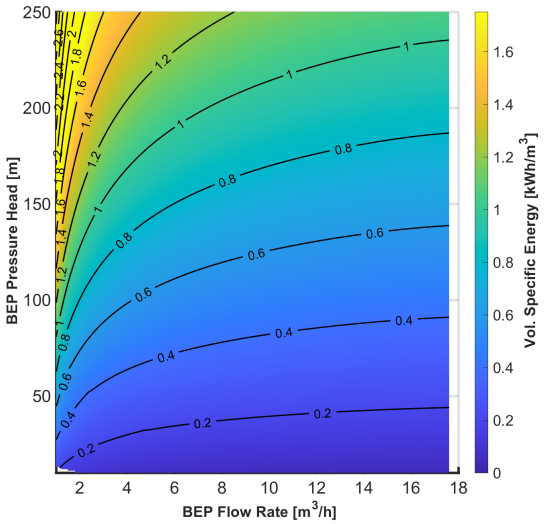

(e) IE2-Driven MSP

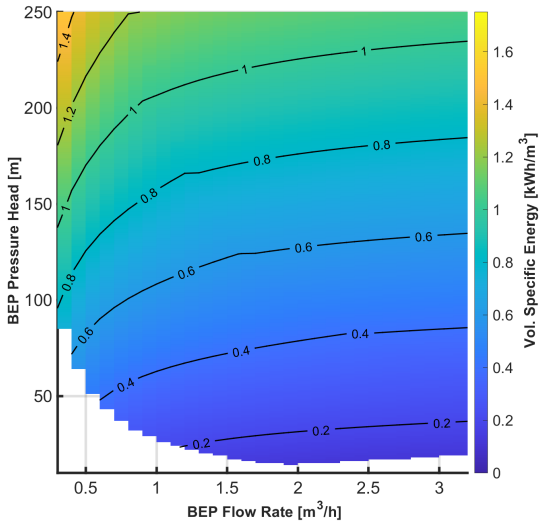

(f) IE2-Driven PCP

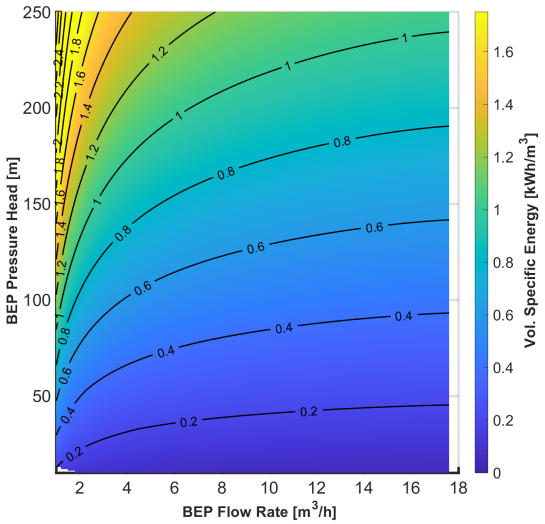

(g) IE3-Driven MSP

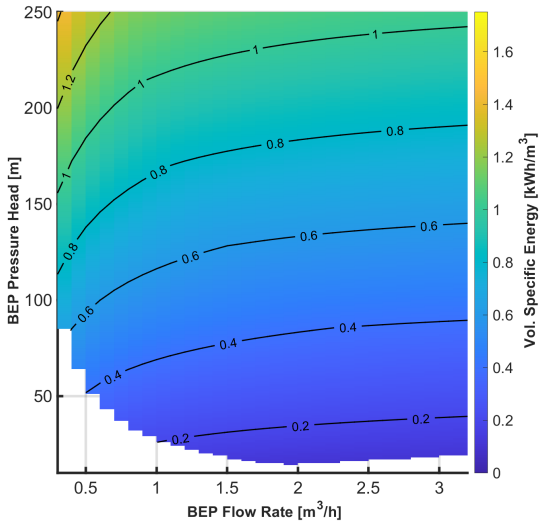

(h) IE3-Driven PCP

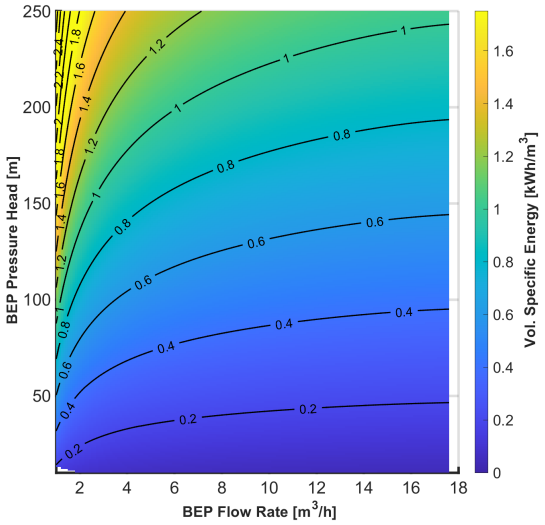

(i) IE4-Driven MSP

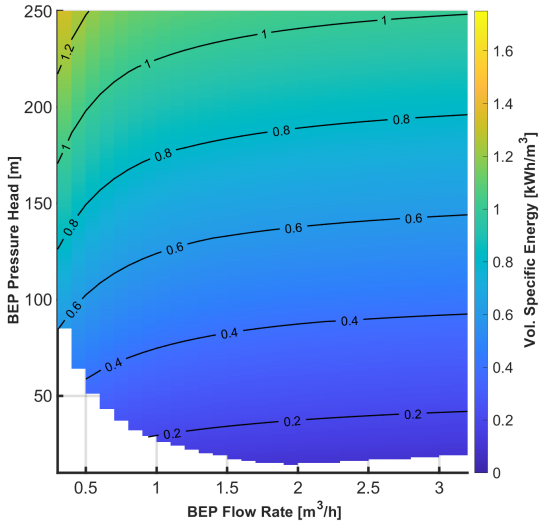

(j) IE4-Driven PCP

Fig. D-1. Volumetric specific energy plots for all listed solar pump architectures listed in Table 3.1, as a function of Q_{BEP} and H_{BEP}.

Appendix E

Tabulated Results of the Operating Point Level Case Study in Section 4.2.

Table E.1. Tabulated results of solar array power and costs for the considered solar pump architectures in the operating point level case study (Section 4.2).

Arch	P_{array}^{hyd}	P_{array}^{pump}	P_{array}^{motor}	P_{array}^{tot}	C_{array}^{hyd}	C_{array}^{pump}	C_{array}^{motor}	C_{array}^{tot}
IM MSP	0.29	0.3	0.42	1.01	236.94	241.36	339.35	817.65
IE1 MSP	0.29	0.3	0.31	0.9	236.94	241.36	253.92	732.22
IE2 MSP	0.29	0.3	0.24	0.83	236.94	241.36	197.79	676.08
IE3 MSP	0.29	0.3	0.2	0.79	236.94	241.36	160.26	638.56
IE4 MSP	0.29	0.3	0.16	0.75	236.94	241.36	126.09	604.38
IM PCP	0.29	0.15	0.37	0.81	236.94	118.07	297.93	652.93
IE1 PCP	0.29	0.15	0.28	0.72	236.94	118.07	224.78	579.78
IE2 PCP	0.29	0.15	0.21	0.65	236.94	118.07	172.46	527.46
IE3 PCP	0.29	0.15	0.17	0.61	236.94	118.07	139.23	494.24
IE4 PCP	0.29	0.15	0.14	0.57	236.94	118.07	110.15	465.16

Solar array power P_{array}^{tot} are in kW_p and the associated array costs C_{array} are in USD.

Bibliography

[1] M. Abdolzadeh and M. Ameri. Improving the effectiveness of a photovoltaic water pumping system by spraying water over the front of photovoltaic cells. *Renewable Energy*, 34(1):91–96, 1 2009.

[2] H. H. Anderson. Prediction of head, quantity and efficiency pumps - the area ratio principle. *Performance Prediction of Centrifugal Pumps and Compressors. ASME*, pages 201–211, 1979.

[3] Jennifer A. Burney and Rosamond L. Naylor. Smallholder Irrigation as a Poverty Alleviation Tool in Sub-Saharan Africa. *World Development*, 40(1):110–123, 1 2012.

[4] Joao Victor Mapurunga Caracas, Guilherme De Carvalho Farias, Luis Felipe Moreira Teixeira, and Luiz Antonio De Souza Ribeiro. Implementation of a high-efficiency, high-lifetime, and low-cost converter for an autonomous photovoltaic water pumping system. *IEEE Transactions on Industry Applications*, 50(1):631–641, 2014.

[5] S. S. Chandel, M. Nagaraju Naik, and Rahul Chandel. Review of solar photovoltaic water pumping system technology for irrigation and community drinking water supplies. *Renewable and Sustainable Energy Reviews*, 49:1084–1099, 2015.

[6] Alvar Closas and Edwin Rap. Solar-based groundwater pumping for irrigation: Sustainability, policies, and limitations. *Energy Policy*, 104:33–37, 2017.

[7] CNP. Nanfang Pump Industry Co,.Ltd., 2020.

[8] Coalition Energy for Access. Global LEAP Awards: 2019 Buyer's Guide for Solar Water Pumps. Technical report, 2019.

[9] Tomás Perpétuo Corrêa, Seleme Isaac Seleme, and Selênio Rocha Silva. Efficiency optimization in stand-alone photovoltaic pumping system. *Renewable Energy*, 41:220–226, 5 2012.

[10] Dayliff. Dayliff - Great Pumps, Great Value, 2020.

[11] Aníbal T De Almeida, Fernando J T E Ferreira, and João Fong. Standards for Efficiency of Electric Motors. 2011.

[12] Jose Gamboa, Aurello Olivet, and Sorelys Espin. New Approach for Modeling Progressive Cavity Pumps Performance. In *Proceedings - SPE Annual Technical Conference and Exhibition*, pages 807–815. Society of Petroleum Engineers, 4 2003.

[13] Meredith Giordano and Charlotte de Fraiture. Small private irrigation: Enhancing benefits and managing trade-offs. *Agricultural Water Management*, 131:175–182, 1 2014.

[14] Grundfos. Grundfos, 2020.

[15] Johann Friedrich Gülich. *Centrifugal Pumps*. Springer, 3 edition, 2014.

[16] IEC. IEC 60034-31-1:2014: Rotating electrical machines - Part 30-1: Efficiency classes of line operated AC motors (IE code), 2014.

[17] IFAD. Smallholders, food security, and the environment. Technical report, International Fund for Agricultural Development, Rome, Italy, 2013.

[18] Nabil Karami, Nazih Moubayed, and Rachid Outbib. General review and classification of different MPPT Techniques. *Renewable and Sustainable Energy Reviews*, 68:1–18, 2 2017.

[19] Igor Karassik, Joseph Messina, Paul Cooper, and Charles Heald. *Pump Handbook*. McGraw Hill, 4 edition, 2008.

[20] Stephen Karekezi and Waeni Kithyoma. Renewable energy strategies for rural Africa: Is a PV-led renewable energy strategy the right approach for providing modern energy to the rural poor to sub-Saharan Africa? *Energy Policy*, 30(11-12):1071–1086, 9 2002.

[21] LORENTZ. Solar Water Pump Systems Manufactured By LORENTZ, 2020.

[22] Sarah K. Lowder, Jakob Skoet, and Terri Raney. The Number, Size, and Distribution of Farms, Smallholder Farms, and Family Farms Worldwide. *World Development*, 87:16–29, 11 2016.

[23] A. M. MacDonald, H. C. Bonsor, B. É Ó Dochartaigh, and R. G. Taylor. Quantitative maps of groundwater resources in Africa. *Environmental Research Letters*, 7(2), 2012.

[24] Dhiaa Halboot Muhsen, Tamer Khatib, and Farrukh Nagi. A review of photovoltaic water pumping system designing methods, control strategies and field performance, 2 2017.

[25] K. Nguyen, T. C. Nguyen, and E. Al-Safran. Modeling the performance of progressive cavity pump under downhole conditions. *Journal of Petroleum Science and Engineering*, 198:108121, 3 2021.

[26] Tan Nguyen. *Artificial Lift Methods: Design, Practices, and Applications Petroleum Engineering*. Springer, 1 edition, 2020.

[27] Tan Nguyen, Eissa Al-Safran, Arild Saasen, and Olav Magnar Nes. Modeling the design and performance of progressing cavity pump using 3-D vector approach. *Journal of Petroleum Science and Engineering*, 122:180–186, 10 2014.

[28] P. Pavelic. *Groundwater availability and use in Sub-Saharan Africa: a review of 15 countries.* International Water Management Institute (IWMI)., 2012.

[29] Paul Pavelic, Karen G. Villholth, Yunqiao Shu, Lisa Maria Rebelo, and Vladimir Smakhtin. Smallholder groundwater irrigation in Sub-Saharan Africa: Country-level estimates of development potential. *Water International*, 38(4):392–407, 7 2013.

[30] Paul Pavelic, Karen G. Villholth, and Shilp Verma. Identifying the barriers and pathways forward for expanding the use of groundwater for irrigation in Sub-Saharan Africa. *Water International*, 38(4):363–368, 7 2013.

[31] Pedrollo. Pedrollo S.p.A | Electric pumps, 2020.

[32] Rolf H. Sabersky, Allan Acosta, Edward G. Hauptmann, and E M Gates. *Fluid Flow: A First Course in Fluid Dynamics*. 1989.

[33] S. Sashidhar and B. G. Fernandes. A low-cost semi-modular dual-stack PM BLDC motor for a PV based bore-well submersible pump. In *Proceedings - 2014 International Conference on Electrical Machines, ICEM 2014*, pages 24–30. Institute of Electrical and Electronics Engineers Inc., 11 2014.

[34] Pulkit Shamshery and Amos G. Winter. Shape and Form Optimization of On-Line Pressure-Compensating Drip Emitters to Achieve Lower Activation Pressure. *Journal of Mechanical Design, Transactions of the ASME*, 140(3), 3 2018.

[35] Julia Sokol, Fiona Grant, Carolyn Sheline, and Amos Winter. Development of a System Model for Low-Cost, Solar-Powered Drip Irrigation Systems in the MENA Region. In *Volume 2B: 44th Design Automation Conference*. American Society of Mechanical Engineers, 8 2018.

[36] Solargis. Global Solar Atlas, 2020.

[37] Gerhard Vetter and Wolfgang Wirth. Understand Progressing Cavity Pumps Characteristics And A Void Abrasive Wear. Technical report, 1995.

[38] Xylem. Xylem Water Solutions & Water Technology | Xylem US, 2020.

[39] Lei Zheng, Xiaodong Wu, Guoqing Han, Huachang Li, Yi Zuo, and Dake Zhou. Analytical Model for the Flow in Progressing Cavity Pump with the Metallic Stator and Rotor in Clearance Fit. *Mathematical Problems in Engineering*, 2018, 2018.